Theor Chem Acc (2007) 117: 7–27
DOI 10.1007/s00214-006-0078-4

REGULAR ARTICLE

Roman F. Nalewajski · Elżbieta Broniatowska

Atoms-in-molecules from the stockholder partition of the molecular two-electron distribution

Received: 10 August 2005 / Accepted: 14 November 2005 / Published online: 30 May 2006

Abstract The effective one-electron distributions of bonded atoms obtained from the "*stockholder*" partition of the molecular two-electron density are reported. These two-electron stockholder (S) atoms are compared with their one-electron analogs represented by the corresponding Hirshfeld (H) one-electron stockholder pieces of the molecular electron density. The influence of the exchange (Fermi) and Coulomb correlation between electrons on the resultant shapes of bonded atoms is investigated The *vertical* (for the fixed molecular electron density) and *horizontal* (involving the electron density displacement) correlation influences on the two-electron stockholder atoms are examined. The two sets of bonded stockholder atoms in the near-dissociation bond-elongated diatomics are compared for different approximations of the electron correlation effects. The cluster components in atomic resolution of the S-partitioning scheme are investigated for illustrative homonuclear and heteronuclear diatomics: H_2, LiH, HF, LiF, and N_2. This framework facilitates an understanding of the origins of the observed differences between the S and H variants of *Atoms-in-Molecules*. With the exception of hydrogen atoms, especially in light molecules, the two sets of bonded atoms were found to be practically identical. For H_2 and LiH the S atoms were shown to exhibit a distinctly higher degree of the bonding character, compared to their H analogs. The main electron correlation effects have been found to be well represented already at the exchange-only level, e.g., in the unrestricted Hartree–Fock (UHF) theory. An inclusion of the extra *vertical* Coulomb correlation exerts a marginal moderating influence on the ionic/covalent composition of the chemical bond already predicted by the UHF approximation, in the direction of a slightly more covalent (less ionic) bond character. The *horizontal* shifts of the molecular density due to Coulomb correlation, relative to the UHF reference, often act in the opposite direction.

R. F. Nalewajski (✉) · E. Broniatowska
Faculty of Chemistry, Jagiellonian University,
R. Ingardena 3, 30-060 Cracow, Poland
E-mail: malewajs@chemia.uj.edu.pl

Keywords Atoms in molecules · Electron correlation · Electron density · Hirshfeld division · Information theory · Stockholder partition · Two-electron distribution

1 Introduction

Fundamental to chemistry is an understanding of molecules as combinations of bonded atoms. It is not surprising that the concept of *Atoms-in-Molecules* (AIM) has been much discussed in the scientific literature (see, e.g., [1–9]) . Let us recall that chemistry deals with small changes of bonded atoms and larger molecular fragments with reasonably well understood and *transferable* molecular invariants such as AIM, functional groups, molecular subsystems, e.g., reactants and products of an elementary chemical reaction, etc., which tend to maintain their identity in different molecular environments. Most molecular systems may be thought of as consisting of only slightly perturbed atoms (or atomic ions), deformed by the presence of the molecular remainder and possibly exhibiting modified net charges. These displacements in the atomic electronic structure are due to the coupled processes of the intra-atomic *polarization* (P) and the inter-atomic *charge transfer* (CT), which accompany the formation of chemical bonds.

Information Theory (IT) [10–21] has recently been demonstrated to provide an attractive framework for an unbiased extraction of such a chemical interpretation from known molecular electron distributions [4–9,22–38]. For example, the Hirshfeld division scheme [3] has recently been shown to have a strong basis in IT [4–9]. This analysis has been extended [6] to cover the related problem of the "stockholder" partition of the many-electron densities in molecular systems. Moreover, the information-theoretic perspective allows one to formulate a thermodynamic-like description of molecules and their constituent parts [22–24] and provides tools for probing the chemical bonds [25–38].

Clearly, the exhaustive partitioning of a given molecular electron density between constituent (bonded) atoms, which determines the AIM effective net charges (oxidation

states) in a given molecular environment, is not unique, since it depends on the adopted criteria for such a division [2]. The Hirshfeld partitioning is also by no means unique, since the two-electron generalization of the underlying stockholder principle [6] is expected to generate slightly different effective one-electron distributions of chemical atoms, which are affected by the electron exchange and Coulomb correlation effects present in the simultaneous electron pair-densities. It is the main goal of the present work to examine these differences in a more detail. The representative diatomics, exhibiting single and multiple chemical bonds of varying degrees of polarization (ionicity), will be investigated using standard quantum theories of electronic structure, both within the wave-function theory [unrestricted Møller-Plessett/Doubles (UHF), MP2] and density functional theory (DFT) [39, 40] (LDA, GGA), by comparing the electron distributions of constituent atoms obtained from the one- and two-electron stockholder divisions. It will be argued that the AIM-cluster components of the two-electron stockholder scheme provide natural channels for the electron redistribution during bond formation. Their implications for the chemical interactions between atoms and reactants in the donor-acceptor complexes will be investigated.

Atomic units are used throughout the article.

2 Stockholder partition of two-electron distributions in diatomics

It has been shown by Hirshfeld [3] that the molecular electron density $\rho(\boldsymbol{r})$ is exhaustively partitioned $\rho(\boldsymbol{r}) = \sum_\alpha \rho_\alpha^H(\boldsymbol{r})$ into the "stockholder" AIM densities $\{\rho_\alpha^H(\boldsymbol{r})\} \equiv \boldsymbol{\rho}^H(\boldsymbol{r})$:

$$\begin{aligned}\rho_\alpha^H(\boldsymbol{r}) &= \rho_\alpha^0(\boldsymbol{r})[\rho(\boldsymbol{r})/\rho^0(\boldsymbol{r})] \equiv \rho_\alpha^0(\boldsymbol{r})\, w\,(\boldsymbol{r}) \\ &= \rho(\boldsymbol{r})[\rho_\alpha^0(\boldsymbol{r})/\rho^0(\boldsymbol{r})] \equiv \rho(\boldsymbol{r}) d_\alpha^H(\boldsymbol{r}), \\ &\sum_\alpha d_\alpha^H(\boldsymbol{r}) = 1. \end{aligned} \tag{1}$$

Here, $\boldsymbol{\rho}^0(\boldsymbol{r}) = \{\rho_\alpha^0(\boldsymbol{r})\}$ groups the densities of the free atoms, giving rise to the reference electron density $\rho^0(\boldsymbol{r}) = \sum_\alpha \rho_\alpha^0(\boldsymbol{r})$ of the (isoelectronic) "promolecule". It consists of the nonbonded constituent atoms shifted to the atomic positions in the molecule. The same promolecular reference is used to determine the familiar density difference function, $\Delta\rho(\boldsymbol{r}) = \rho(\boldsymbol{r}) - \rho^0(\boldsymbol{r})$, which extracts changes in the electron distribution due to the chemical bonds. A reference to Eq. (1) shows that Hirshfeld AIM densities satisfy the local one-electron *stockholder principle*, which can be stated as the following equality between the molecular and promolecular conditional probabilities, $\pi^H(\alpha|\boldsymbol{r})$ and $\pi^0(\alpha|\boldsymbol{r})$, respectively, that an electron localized at $\boldsymbol{r}$ originates from atom α:

$$\begin{aligned} d_\alpha^H(\boldsymbol{r}) &= \rho_\alpha^H(\boldsymbol{r})/\rho(\boldsymbol{r}) \equiv \pi^H(\alpha|\boldsymbol{r}) \\ &= d_\alpha^0(\boldsymbol{r}) = \rho_\alpha^0(\boldsymbol{r})/\rho^0(\boldsymbol{r}) \equiv \pi^0(\alpha|\boldsymbol{r}). \end{aligned} \tag{2}$$

It has been interpreted by Hirshfeld using the stock market analogy that each atom participates locally in the molecular "profit" $\rho(\boldsymbol{r})$ in proportion to its share $d_\alpha^0(\boldsymbol{r})$ in the promolecular "investment" $\rho^0(\boldsymbol{r})$. This scheme has been validated using the minimum principle of the entropy deficiency [17,18] between the electron distributions of the bonded and free atoms subject to the local constraint of the exhaustive partition of the molecular electron density [4–9]. It also follows from Eq. (1) that in this one-electron stockholder scheme each free subsystem density is locally modified in accordance with the *molecular* (subsystem independent) density *enhancement factor* $w(\boldsymbol{r})$. Therefore, this procedure is devoid of any subsystem bias and as such appears to be fully objective.

This one-electron division rule has been generalized into the corresponding many-electron principle [6]. We shall illustrate this extended partitioning for the most important *two*-electron case. As an illustrative example let us consider a diatomic molecule $M = A$–B containing N electrons. For diatomics the stockholder division of the molecular joint two-electron probability distribution $p_2(\boldsymbol{r}, \boldsymbol{r}')$ of simultaneously finding two electrons at indicated positions or the corresponding electron pair-density $\rho_2(\boldsymbol{r}, \boldsymbol{r}') = N(N-1)p_2(\boldsymbol{r}, \boldsymbol{r}')$, involves four components corresponding to different pairs of atoms from which the two electrons originate, here called the *AIM two-clusters* [6]:

$$\begin{aligned} \mathbf{p}^S(\boldsymbol{r}, \boldsymbol{r}') &= \{p_{\alpha\beta}^S(\boldsymbol{r}, \boldsymbol{r}')\}, \\ \boldsymbol{\rho}_2^S(\boldsymbol{r}, \boldsymbol{r}') &= \{\rho_{\alpha\beta}^S(\boldsymbol{r}, \boldsymbol{r}') = N(N-1)p_{\alpha\beta}^S(\boldsymbol{r}, \boldsymbol{r}')\}, \\ p_2(\boldsymbol{r}, \boldsymbol{r}') &= \sum_{\alpha=A,B}\sum_{\beta=A,B} p_{\alpha\beta}^s(\boldsymbol{r}, \boldsymbol{r}'), \\ \rho_2(\boldsymbol{r}, \boldsymbol{r}') &= \sum_{\alpha=A,B}\sum_{\beta=A,B} \rho_{\alpha\beta}^S(\boldsymbol{r}, \boldsymbol{r}'). \end{aligned} \tag{3}$$

These four pieces of the molecular two-electron probability distribution are defined by the *two-electron stockholder principle*:

$$\begin{aligned} &p_{\alpha\beta}^S(\boldsymbol{r}, \boldsymbol{r}') \\ &\quad = p_{\alpha\beta}^0(\boldsymbol{r}, \boldsymbol{r}')/p_2^0(\boldsymbol{r}, \boldsymbol{r}')]p_2(\boldsymbol{r}, \boldsymbol{r}') \equiv d_{\alpha\beta}^S(\boldsymbol{r}, \boldsymbol{r}')p_2(\boldsymbol{r}, \boldsymbol{r}') \\ &p_{\alpha\beta}^S(\boldsymbol{r}, \boldsymbol{r}') = [p_{\alpha\beta}^0(\boldsymbol{r}, \boldsymbol{r}')/p_2^0(\boldsymbol{r}, \boldsymbol{r}')]p_2(\boldsymbol{r}, \boldsymbol{r}') \\ &\quad \equiv w_2(\boldsymbol{r}, \boldsymbol{r}')p_{\alpha\beta}^0(\boldsymbol{r}, \boldsymbol{r}'), \end{aligned} \tag{4}$$

where the reference, two-electron probability distribution of the isoelectronic promolecule, is the sum of promolecular contributions $\{p_{\alpha\beta}^0(\boldsymbol{r}, \boldsymbol{r}')\}$ from the free-atom clusters, $p_2^0(\boldsymbol{r}, \boldsymbol{r}') = \sum_{\alpha=A,B}\sum_{\beta=A,B} p_{\alpha\beta}^0(\boldsymbol{r}, \boldsymbol{r}')$, $d_{\alpha\beta}^S(\boldsymbol{r}, \boldsymbol{r}')$ stands for the two-electron *share factor* (conditional probability) of the (α, β)-cluster,

$$\begin{aligned} d_{\alpha\beta}^S(\boldsymbol{r}, \boldsymbol{r}') &= [p_{\alpha\beta}(\boldsymbol{r}, \boldsymbol{r}')/p_2(\boldsymbol{r}, \boldsymbol{r}')] \equiv \pi_2^S(\alpha, \beta|\boldsymbol{r}, \boldsymbol{r}') \\ &= d_{\alpha\beta}^0(\boldsymbol{r}, \boldsymbol{r}') = [p_{\alpha\beta}^0(\boldsymbol{r}, \boldsymbol{r}')/p_2^0(\boldsymbol{r}, \boldsymbol{r}')] \\ &\equiv \pi_2^0(\alpha, \beta|\boldsymbol{r}, \boldsymbol{r}'), \end{aligned} \tag{5}$$

and $w_2(\boldsymbol{r}, \boldsymbol{r}')$ denotes the universal (molecular, cluster-independent) *enhancement factor* for the specified positions of the two electrons. Therefore, Eq. (4) again predicts that

each AIM 2-cluster partakes in the two-electron molecular "profit" $p_2(\boldsymbol{r},\boldsymbol{r}')$ in proportion to its share $d^0_{\alpha\beta}(\boldsymbol{r},\boldsymbol{r}')$ in the promolecular "investment" $p^0_2(\boldsymbol{r},\boldsymbol{r}')$.

There are the two *atomic* (diagonal, $\alpha=\beta$) and two *diatomic* (off-diagonal, $\alpha\neq\beta$) contributions in Eq. (3). Their share factors are proportional to the corresponding reference distributions $\mathbf{p}^0(\boldsymbol{r},\boldsymbol{r}')=\{p^0_{\alpha\beta}(\boldsymbol{r},\boldsymbol{r}')\}$ of the free atoms:

$$p^0_{\alpha\beta}(\boldsymbol{r},\boldsymbol{r}')=\{p^0_{2,\alpha}(\boldsymbol{r},\boldsymbol{r}'),\ \alpha=\beta;\quad p^0_\alpha(\boldsymbol{r})p^0_\beta(\boldsymbol{r}'),\ \alpha\neq\beta\},\tag{6}$$

where $p^0_\alpha(\boldsymbol{r})$ and $p^0_{2,\alpha}(\boldsymbol{r},\boldsymbol{r}')$ denote the one-electron and (joint) two-electron probability densities of the free atom α.

The kernels $\mathbf{p}^S(\boldsymbol{r},\boldsymbol{r}')$ or $\boldsymbol{\rho}^S_2(\boldsymbol{r},\boldsymbol{r}')$ or their partially integrated, effective one-electron components

$$\mathbf{p}^{\rm eff}(\boldsymbol{r})=\int\mathbf{p}^S(\boldsymbol{r},\boldsymbol{r}')\mathrm{d}\boldsymbol{r}'=\{p^{\rm eff}_{\alpha\beta}(\boldsymbol{r})\},$$
$$\boldsymbol{\rho}^{\rm eff}(\boldsymbol{r})=\int\boldsymbol{\rho}^S_2(\boldsymbol{r},\boldsymbol{r}')\mathrm{d}\boldsymbol{r}'=\{\rho^{\rm eff}_{\alpha\beta}(\boldsymbol{r})\},\tag{7}$$

define the effective one-electron density of bonded atoms:

$$\sum_{\beta=A,B}\rho^{\rm eff}_{\alpha\beta}(\boldsymbol{r})=\rho^{\rm eff}_\alpha(\boldsymbol{r}),\quad \alpha=A,B.\tag{8}$$

In what follows we shall compare examples of such atomic electron densities with the corresponding Hirshfeld pieces of the molecular one-electron distribution. They define two sets of AIM, which we shall call the 2-*S* and 1-*S* (Hirshfeld) bonded atoms, respectively. The 2-*S* atoms, which are explicitly electron-correlation dependent, can be expected to generate the effective one-electron distributions, which slightly differ from the corresponding Hirshfeld (1-*S*) densities, since the two sets of bonded atoms are obtained from partitioning different physical quantities.

3 Electron distributions of the one-and two-electron stockholder atoms

3.1 Computational details

The effective one-electron densities $\rho^{\rm eff}_\alpha(\boldsymbol{r})$ of the 2-*S* AIM $\left(\alpha^S\right)$ and the electron densities $\rho^H_\alpha(\boldsymbol{r})$ of the Hirshfeld 1-*S* bonded atoms (α^H), will be compared for H_2, LiH, HF, LiF, and N_2 These molecules cover the purely covalent bonds, single in H_2 and triple in N_2, as well as the partly ionic bonds in the remaining heteronuclear diatomics. This selection allows one to examine the effect of a growing number of the open two-electron channels (AIM two-clusters) in the 2-*S* partitioning procedure: two off-diagonal channels in H_2, one diagonal and two off-diagonal channels in LiH and HF, and all four channels (two diagonal and two off-diagonal) in N_2 and LiF.

The numerical results will be generated using standard UHF, UHF + MP2 ≡ UMP2 and Kohn–Sham (KS) DFT (KS/LDA and KS/B3LYP) calculations in the extended (DZV or DZVP) basis sets, which involve the split-valence atomic orbitals (DZV), in some calculations supplemented by the polarization functions (DZVP). This analysis has been performed for several internuclear separations ranging from the equilibrium bond length to the near-dissociation distances. The AIM densities will also be compared with the corresponding reference densities $\boldsymbol{\rho}^0(\boldsymbol{r})$ of the separated (free) constituent atoms. The equilibrium geometries in the adopted basis sets have been used. In order to precisely separate the Coulomb correlation effects on effective AIM distributions, the common UHF equilibrium geometry has been used in the 1-*S* and 2-*S* partitions.

In the present analysis we are interested in differences in the effective one-electron distributions of the two-electron stockholder (2-*S*) AIM relative to those characterizing the Hirshfeld (1-*S*) bonded atoms, which give rise to the *same* molecular electron density ρ. In order to facilitate such a comparison, the constraint of the fixed density $\rho=\rho^{\rm UHF}$ was imposed in the UMP2 numerical calculations. It should be realized, however, that the same electron density and external potential in both these partition schemes in DFT imply the same molecular electronic energies corresponding to the two sets of constituent atoms. Therefore, only the "*vertical*" (for the identical electron densities) influence of the Coulomb correlation holes on the resultant electron distributions of 2-*S* AIM, estimated using the MP2 theory for the fixed, Coulomb-uncorrelated molecular electron density, was examined.

Clearly, the Coulomb-correlated calculations ultimately give rise to the optimum electron density, which is slightly modified relative to the UHF result, $\rho^{\rm UMP2}\neq\rho^{\rm UHF}$, by what we call the "*horizontal*" displacement in the system electronic structure. This change in the equilibrium distribution of electrons lowers the system electronic energy by the Coulomb-correlation energy: $E^{\rm UMP2}-E^{\rm UHF}=\Delta E_{\rm c}<0$. The corresponding expression for the electron pair-density in terms of the exchange-correlation (xc) hole $h^{\rm UMP2}_{\rm xc}(\boldsymbol{r}'|\boldsymbol{r})$ gives the following partition into the independent-particle (Hartree, *H*) contribution and the correlation corrections due to the Fermi (*x*) and Coulomb (*c*) holes, respectively:

$$\begin{aligned}\rho^{\rm UMP2}_2(\boldsymbol{r},\boldsymbol{r}')&=\rho^{\rm UMP2}(\boldsymbol{r})\left[\rho^{\rm UMP2}(\boldsymbol{r}')+h^{\rm UMP2}_{xc}(\boldsymbol{r}'|\boldsymbol{r})\right]\\&\equiv\rho^{\rm UMP2}_{2,H}(\boldsymbol{r},\boldsymbol{r}')+\rho^{\rm UMP2}_{2,xc}(\boldsymbol{r},\boldsymbol{r}')\\&=\{\rho^{\rm UMP2}(\boldsymbol{r})\left[\rho^{\rm UMP2}(\boldsymbol{r}')+h^{\rm UMP2}_x(\boldsymbol{r}'|\boldsymbol{r})\right]\\&\quad+h^{\rm UMP2}_c(\boldsymbol{r}'|\boldsymbol{r})\}\\&\equiv\rho^{\rm UMP2}_{2,Hx}(\boldsymbol{r},\boldsymbol{r}')+\rho^{\rm UMP2}_{2,c}(\boldsymbol{r},\boldsymbol{r}').\end{aligned}\tag{9}$$

Above, we have used the familiar partition of the resultant hole into the separate exchange (*x*) and (Coulomb) correlation (*c*) contributions. Here, the subscript *Hx* symbolizes the sum of the Hartree and exchange contributions.

The present analysis of the "vertical" (fixed-density) correlation effects in the 2-*S* partition of the UHF density is done by approximating in the foregoing equation $\rho^{\rm UMP2}(\boldsymbol{r})\cong\rho^{\rm UHF}(\boldsymbol{r})$ and hence also

$$\rho^{\rm UMP2}_{2,H}(\boldsymbol{r},\boldsymbol{r}')\cong\rho^{\rm UHF}_{2,H}(\boldsymbol{r},\boldsymbol{r}')\quad\text{and}$$
$$\rho^{\rm UMP2}_{2,Hx}(\boldsymbol{r},\boldsymbol{r}')\cong\rho^{\rm UHF}_2(\boldsymbol{r},\boldsymbol{r}'),\tag{10}$$

since the UHF MO have been used in the subsequent MP2 procedure for estimating the Coulomb-hole. These approximations give the following final expression for the electron pair-density, which constitutes the basis of the present, "vertical" analysis:

$$\rho_2^{\mathrm{UMP2}}(\boldsymbol{r},\boldsymbol{r}') \approx \rho_2^{\mathrm{UHF}}(\boldsymbol{r},\boldsymbol{r}') + \rho^{\mathrm{UHF}}(\boldsymbol{r}) h_c^{\mathrm{UMP2}}(\boldsymbol{r}'|\boldsymbol{r}). \quad (11)$$

It can be straightforwardly verified using the familiar sum rules satisfied by the correlation holes, that the integration over $\boldsymbol{r}'$ indeed recovers $\rho^{\mathrm{UHF}}(\boldsymbol{r}) = (N-1)^{-1}\int \rho_2^{\mathrm{UHF}}(\boldsymbol{r},\boldsymbol{r}')\,\mathrm{d}\boldsymbol{r}'$ since the second Coulomb-correlation contribution exactly vanishes: $\int h_c^{\mathrm{UMP2}}(\boldsymbol{r}'|\boldsymbol{r})\mathrm{d}\boldsymbol{r}' = 0$.

The familiar antisymmetry requirement imposed on the N-electron wave-function implies the statistical, *exchange* (x) correlation between the movements of like-spin electrons. In our approximation, the two-electron conditional probabilities, which take into account this Pauli *exclusion principle*, describe the *non-interacting* system of the *same* electron density as that of the *real* system consisting of fully *interacting* electrons. These joint two-electron probabilities, which carry the exchange correlation, are fully determined by the KS orbitals. Since in the KS limit, for the vanishing coupling constant in the adiabatic connection of DFT, the *Coulomb* (c) correlation due to finite charges of electrons is completely turned off, the Fermi correlation accounts for the whole correlation of the non-interacting system. In the *real* system, of the fully *interacting* electrons, the KS orbitals determine only the x-holes of the resultant xc-holes characterizing the total correlation effects in molecular systems.

The UHF approximation, which in principle can be regarded as roughly equivalent to the exact-exchange-only DFT scheme, has been selected to generate the reference data, which exhibit the correct behavior in the dissociation limit. Since the correlation effects in typical DFT methods are only correct at the level of the average correlation holes, we have limited the DFT analysis to the KS (non-interacting) limit, which exclusively covers the exchange effects embodied in the two-electron probabilities generated by the KS molecular orbitals. We denote such an UHF-like approach as the UHF-KS scheme. Indeed the results obtained for molecules in UHF and UHF-KS approximations will be shown to be practically indistinguishable. Only at internuclear distances close to bond dissociation, does one detect appreciable differences due to a general inadequacy of the UHF-KS inter-atomic exchange holes in such bond-elongated systems, both in the LDA and GGA/B3LYP variants. The effects of the Coulomb correlation will be determined using the spin-unrestricted Møller–Plessett (MP) theory (UMP2), which takes into account the double excitations from the UHF ground-state electron configuration.

3.2 Vertical effects of the electron correlation

Figure 1 compares the bond profiles of the molecular and atomic electron densities in H_2 and LiH. The reported UHF plots are also representative of the UHF-KS (LDA and B3LYP) results in the same basis sets which are practically

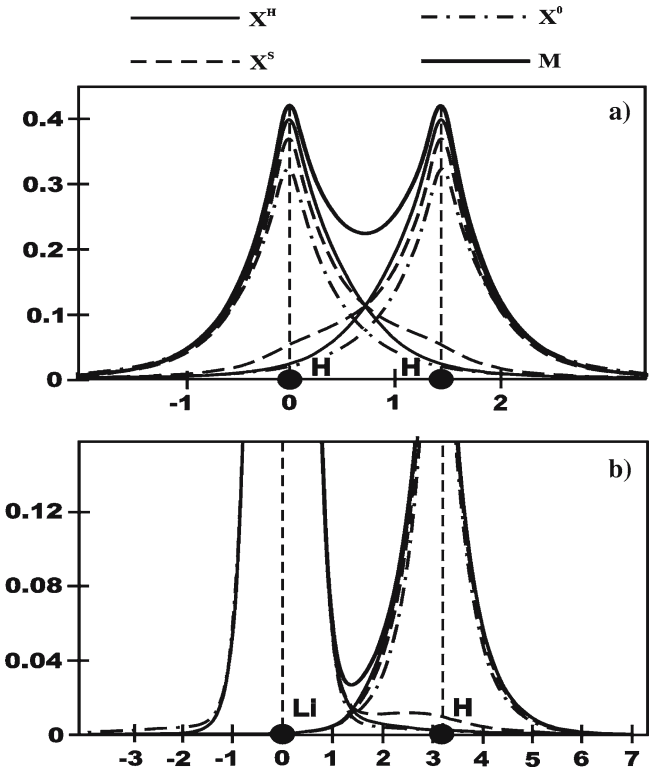

Fig. 1 A comparison of the molecular $\rho(\boldsymbol{r})[M]$ and atomic, $\rho_\alpha^0(\boldsymbol{r})[\alpha^0]$, $\rho_\alpha^{\mathrm{eff}}(\boldsymbol{r})[\alpha^S]$, and $\rho_\alpha^H(\boldsymbol{r})[\alpha^H]$, electron densities in H_2 (**a**)*and LiH* (**b**) obtained from the unrestricted Hartree–Frock calculations. The associated plots generated by the density functional theory calculations in the LDA and B3LYP approximations (UHF-Kohn–Sham (KS) scheme) are practically indistinguishable from the reported UHF results (DZVP basis set). Equilibrium bond lengths have been assumed and atomic units are used throughout

indistinguishable for the equilibrium bond lengths assumed in the figure. It follows from panel a of the figure, that in H_2 both the H^S (2-S) and H^H (1-S) atoms assume a distinct molecular character, being polarized towards the bonding partner and exhibiting the extra contraction near the nucleus, in comparison to the spherical probability distribution of the free hydrogen. However, the two profiles of the bonded hydrogen atoms are quite different. The effective probability plot from the two-electron stockholder distribution extends more strongly towards the other atom, thus penetrating more effectively the bonding region of the molecule at the expense of the area around the atomic nucleus, where a weaker contraction can be detected. In H_2, due to the one-electron reference of the neutral hydrogen, only the two off-diagonal contributions, which we call "covalent" by analogy to the valence-bond (VB) structures of the Heitler–London theory of the chemical bond [41–43], participate in the two-electron stockholder division. The exactly vanishing diagonal ("ionic") channels imply that the deviations between 1-S and 2-S densities observed in Fig. 1a for such a *Hard–Hard* diatomic are solely of the "covalent" origin.

These observations hold true in LiH as well (see Fig. 1b), in which the extra diagonal ("ionic") channel on Li opens in the 2-S partitioning. In this molecule the largest deviations

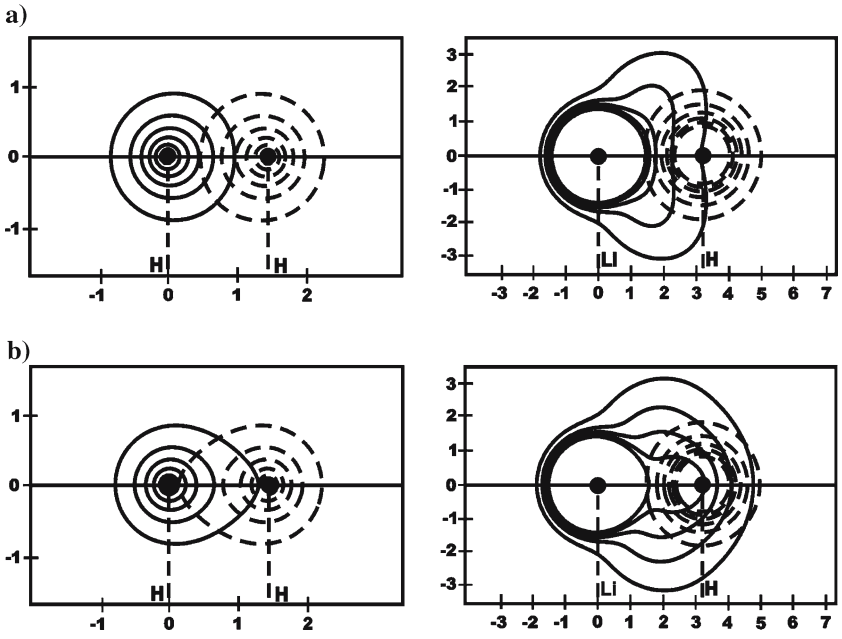

Fig. 2 A comparison of the contour diagrams of the $\rho_\alpha^H(\boldsymbol{r})$ (**a**) and $\rho_\alpha^{\text{eff}}(\boldsymbol{r})$ (**b**) distributions of bonded atoms in H_2 (*left column*) and LiH (*right column*) from the UHF calculations. The associated DFT (UHF-KS) plots in the LDA and B3LYP approximations are practically indistinguishable from the reported UHF diagrams. The equilibrium bond lengths have been assumed (DZVP basis set)

between the 1-*S* and 2-*S* electron distributions can be detected on Li. Indeed, in this *Soft*(Li)–*Hard*(H) molecule the effective density of the heavy atom contains both the diagonal (*ionic*) and a weak off-diagonal (*covalent*) contributions, while the hydrogen electron density contains only a small *covalent* part. We shall demonstrate in Sect. 4 that the bonding "shoulder" of the Li effective distribution in Fig. 1b is due to the off-diagonal (covalent) [Li,H]-contribution. It is seen to extend well into the region around the hydrogen nucleus.

The contour maps reported in Fig. 2 further illustrate the extra-bonding character of the 2-*S* AIM, compared to the Hirshfeld (1-*S*) bonded atoms in these two molecules. Indeed, in the H_2 case the 2-*S* hydrogen exhibits a stronger cylindrical polarization around the bond axis, compared to the weakly polarized, almost spherical 1-*S* (Hirshfeld) atom. In LiH the *acceptor* (hydrogen) atom is seen to remain almost spherical in both one- and two-electron stockholder division schemes, while the *donor* (Li) atom is seen to be more strongly polarized towards the hydrogen in the 2-*S* partition. In this molecule the density contours of the heavier atom Li^S exhibit a distinct directional character. This feature is lacking in Li^H, in the one-electron (Hirshfeld) division, where the directions of the maximum polarization are seen to lie on the surface of the cone at roughly an angle of 45° relative to the Li–H bond axis.

A similar comparison of the contour maps and density profiles for constituent atoms in HF (Fig. 3) reveals that there are no appreciable differences between the 1-*S* and 2-*S* stockholder AIM in this heavier molecule. Therefore, with a growing number of the valence electrons, the subtle differences in the shapes of the stockholder AIM due to the electron correlation gradually disappear. The same general conclusion follows from examining the logarithmic AIM density plots in N_2 and LiF, which we shall report in Sect. 4. For the equilibrium internuclear distance the differences between the 1-*S* and 2-*S* in one-electron distributions of bonded atoms in these

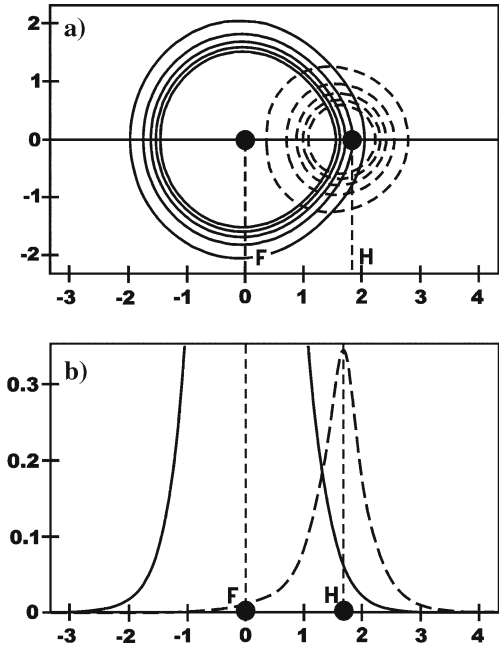

Fig. 3 Contour diagrams (**a**) of the effective electron density of the 2-*S* AIM and the electron densities of the 1-*S* (Hirshfeld) atoms (both plots are indistinguishable in the scale of the figure) in HF (UMP2 approximation), together with the corresponding bond-axis profiles (**b**) (DZV basis set)

systems practically disappear. Thus, in heavier molecules the 1-*S* and 2-*S* stockholder AIM become for all practical purposes identical.

In Fig. 4 we have examined in more detail the effect of the electron correlation on the effective density profiles of 2-*S* bonded atoms in H_2 and LiH. A reference to panel a of the figure shows that the bonding shoulder of the 2-*S* hydrogen atom in H_2 is only slightly lowered and there is slightly more density contraction in the vicinity of the nucleus when one turns on the Coulomb correlation on top of the exact exchange. A higher bonding character of the 2-*S* AIM relative to the 1-S bonded atom is again clearly seen in this density profile.

The same general conclusion follows from examining panel b of the figure. The inclusion of the Coulomb correlation slightly lowers the bonding part of the density profile of the bonded 2-*S* Li atom in comparison to the exchange-only plot. This blow-up picture emphasizes the bonding region where the differences between the 2-*S* and 1-*S* profiles are most apparent. However, as the corresponding hydrogen plots

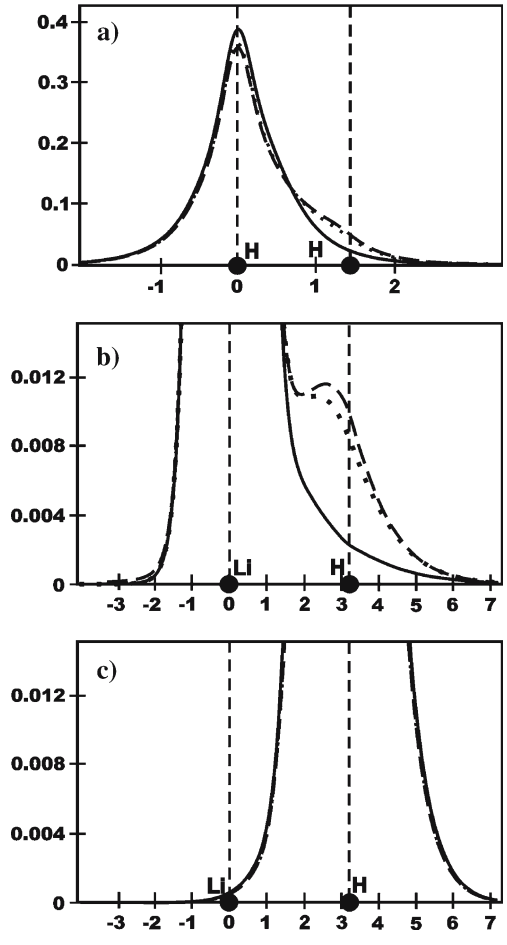

Fig. 4 The effect of the exchange (UHF, *broken line*) and Coulomb (UMP2, *dotted line*) electron correlation on the bond-axis profiles of the effective electron densities of 2-*S* AIM in H_2 (**a**) and LiH (**b**, **c**). The 1-*S* (Hirshfeld, *solid line*) plots are also shown for comparison (DZV basis set)

of panel c and Fig. 1b clearly show, the overall distributions of the 2-*S* and 1-*S* are not that very different. With the exception of the bonding region the two profiles are almost identical. This closeness of the two sets of the bonded stockholder atoms becomes even stronger in diatomics consisting of two heavy atoms, e.g., LiF and N_2, in which all four two-electron channels (AIM two-clusters) become available for the stockholder partitioning of the molecular pair-density (see Sect. 4).

The details of generally minor local differences between the effective electron distributions of the 2-*S* AIM, relative to the electron densities of the 1-*S* (Hirshfeld) atoms in all five representative diatomics are displayed in the *left column* of Fig. 5, where the relevant *difference* profiles are displayed. As expected, these deviations decay fast with the growing number of electrons from H_2 ($N = 2$) to N_2 ($N = 14$). The largest differences, observed in panel a, indicate that the 2-*S* bonded hydrogens in H_2 shift the electron density from the non-bonding and nuclear regions towards the other nucleus, relative to the corresponding Hirshfeld atomic pieces of the molecular electron density.

A different pattern of such AIM density relocations due to the electron correlation is observed in heteronuclear diatomics of panels b, c, and d of the left column in the figure. In LiH (panel b) the lithium atom gains electrons at the expense of hydrogen atom, with the maximum of these deviations being observed near the nucleus of a more electronegative (harder) hydrogen atom. This polarization shows that the 2-*S* AIM slightly lower the charge separation exhibited by the net charges of the Hirshfeld AIM reported in Table 1.

Similar deviations are exhibited by the difference plots of panel c for HF, which are limited basically to the bonding region between the two nuclei. This time the positively charged 2-*S* hydrogen atom gains electrons relative to the corresponding Hirshfeld density, while the negatively charged fluorine atom loses part of its excess electron density. Thus again the 2-*S* partition partly moderates the AIM charge separation generated by the 1-*S* partition. A reference to panel d shows the same effect in LiF, although the magnitude of the maximum density difference is now ten times lower.

A more complex redistribution pattern is found for N_2 (panel e). The 2-*S* nitrogen atom, when compared with its 1-*S* analog, is seen to slightly shift its valence electrons from both the non-bonding and bonding regions to the valence shell of the other nitrogen. Therefore, the electron correlation delicately increases the bonding character of the two-electron stockholder nitrogens in comparison to the Hirshfeld (1-*S*) subsystems. However, as witnessed by the magnitude of the density oscillations, comparable to those observed in LiF, this change is so minute that it is practically invisible in the absolute density plots.

Next, let us examine the resolution of these overall correlation-induced differences between the 1-*S* and 2-*S* AIM, repeated as broken-line profiles in the right column in Fig. 5, into contributions due to the exchange (solid line) and Coulomb (dotted line) correlation effects. This partition is shown in the *right* column of Fig. 5. A general conclusion following

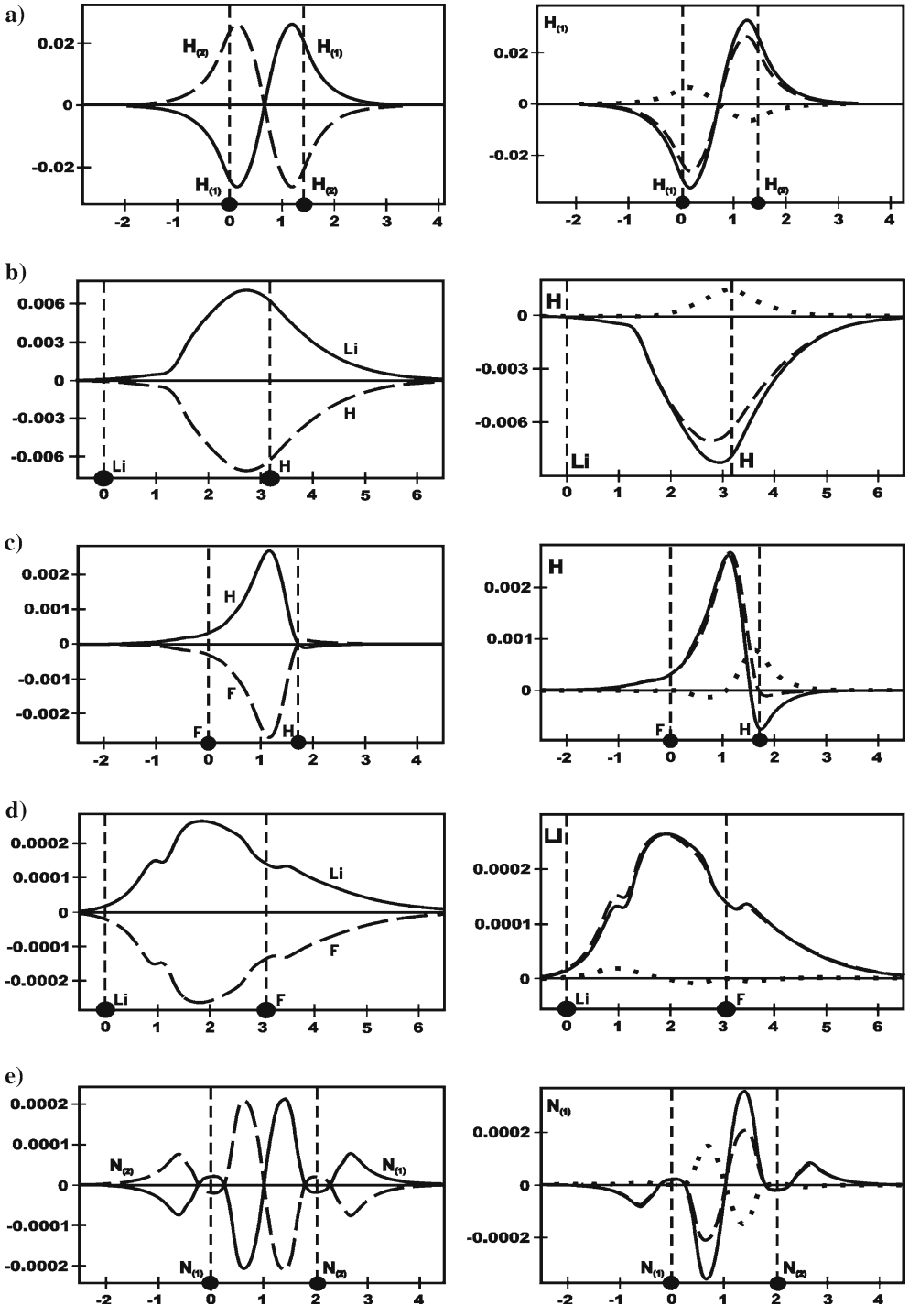

Fig. 5 *Left column*: deviations between the densities $\{\rho_\alpha^{\mathrm{eff}}(\boldsymbol{r})\}$ of the 2-*S* AIM and $\{\rho_\alpha^{H}(\boldsymbol{r})\}$ of the 1-*S* bonded atoms along the bond axis (DZV basis set, UMP2 approximation). *Right column* plots provide a resolution of the overall displacements (*broken line*) into the corresponding shifts due to the Fermi (exchange, *solid line*) and Coulomb (*dotted line*) correlation between electrons. Molecules: H_2 (**a**), LiH (**b**), HF (**c**), LiF (**d**), and N_2 (**e**)

from these density difference profiles is that the Coulomb correlation slightly moderates the displacements due to the Pauli exclusion principle with the density oscillations due to Coulomb correlation exhibiting opposite phase in comparison to the corresponding exchange curves. The Fermi correlation contribution dominates the overall displacements and gives rise to a slightly stronger bonding character of the effective electron densities of the 2-*S* atoms, while the Coulomb correlation influence makes the shape of the 2-*S* AIM closer to that of the Hirshfeld atoms.

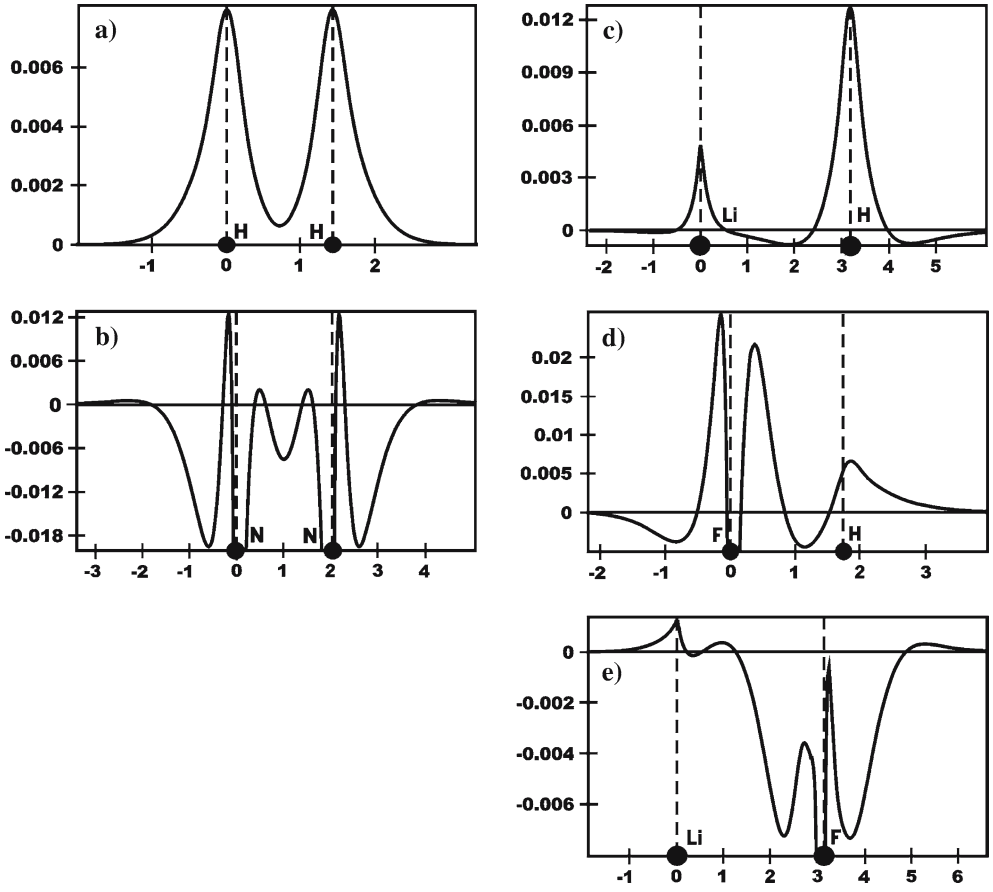

Fig. 6 The "horizontal" shifts in the molecular electron density due to the Coulomb correlation, $\Delta\rho^{\text{horizontal}} = \rho^{\text{UMP2}} - \rho^{\text{UHF}}$, for selected homonuclear diatomics (*left column*), H_2 (**a**), N_2 (**b**), and heteronuclear diatomic molecules (*right column*), LiH (**c**), HF (**d**), and LiF (**e**)

Table 1 A comparison of the net charges (a.u.) of the bonded AIM in LiH, HF, and LiF, obtained from the one-electron (H) and two-electron (S) stockholder division of the molecular electron distributions (density functional theory LDA calculations, DZVP basis set). The 2-S AIM have been generated using the two-electron joint probabilities generated by the KS orbitals (Unrestricted Hartree–Fock scheme)

Molecule	AIM (α)	q_α^H	q_α^S
LiH	Li	0.35	0.24
HF	H	0.24	0.21
LiF	Li	0.58	0.56

3.3 Horizontal density displacements due to the Coulomb correlation

It should be emphasized that this development takes into account only the "vertical" correlation influence on the resulting densities of 2-S AIM,

$$\Delta\boldsymbol{\rho}^{\text{vertical}} = \boldsymbol{\rho}^S(\rho)^{\text{UMP2}} - \boldsymbol{\rho}^S(\rho)^{\text{UHF}},$$

for the fixed molecular one-electron distribution ρ, common to both the 1-S and 2-S partitions. However, an inclusion of the Coulomb correlation changes the system electron density relative to the UHF treatment. This "horizontal" correlation influence further affects both the Hirshfeld and two-electron stockholder AIM.

In Fig. 6 we have examined the horizontal shifts of the *molecular* electron density due to the Coulomb correlation,

$$\Delta\rho^{\text{horizontal}} = \rho^{\text{UMP2}} - \rho^{\text{UHF}},$$

for all five diatomics considered in the present analysis. Their Hirshfeld components are displayed in Fig. 7.

A reference to Fig. 6a shows that the Coulombic part of the electron correlation shifts the electron density from the far-outside regions of the UHF molecular distribution towards the nuclei and, to a lesser degree, to the bonding region between them. This pattern should indeed be intuitively expected, since the two spin-paired electrons occupying the bonding MO are not Fermi-correlated so that their close, near-coalescence encounters are not excluded by the Pauli principle. Therefore, the inclusion of the Coulomb correlation between the two electrons will be felt most strongly in the regions of the highest electron concentration, i.e., near the nuclei and in the bonding region. Since the correlation avoidance of two electrons effectively increases the average distance between them thus lowering their repulsion, one should expect a slight inflow into these regions of the highest accumulation of the UHF electron density in the molecule.

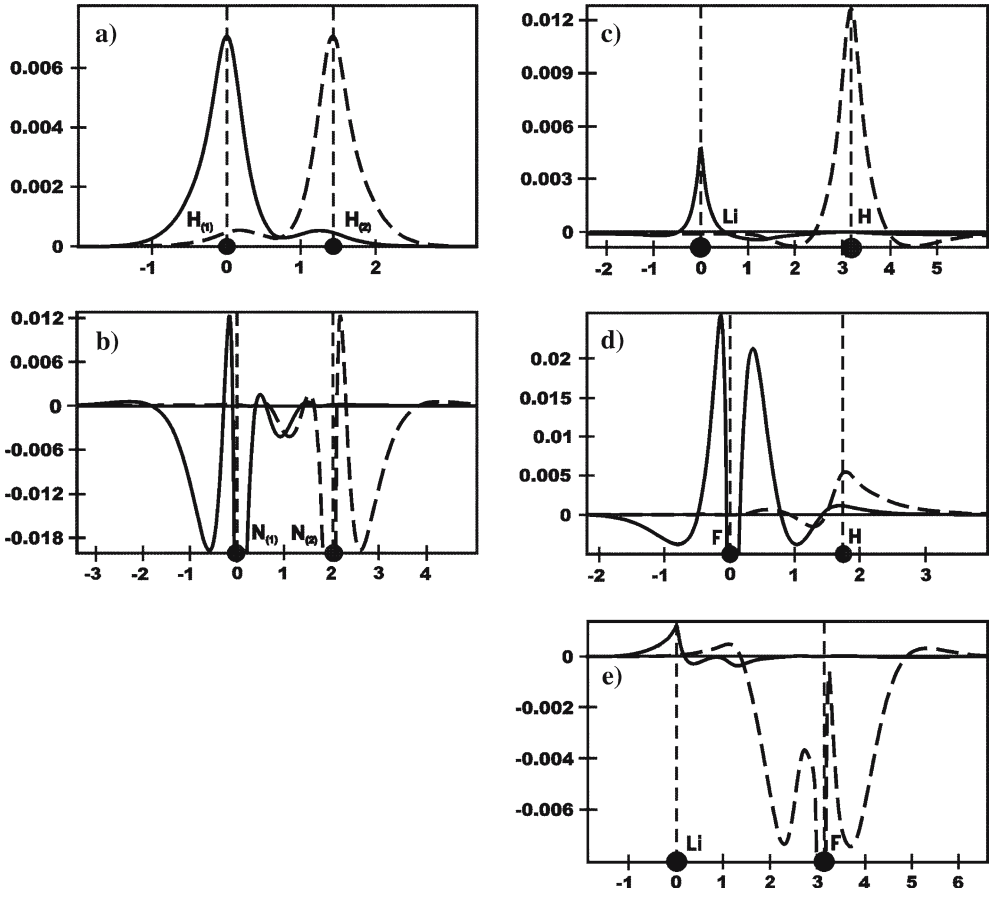

Fig. 7 The "horizontal" shifts in the electron densities of the Hirshfeld AIM in diatomic molecules of Fig. 6 due to the Coulomb correlation: $\Delta\rho_X^{H,\text{horizontal}} = \rho_X^{H,\text{UMP2}} - \rho_X^{H,\text{UHF}}$. These diagrams provide the 1-S atomic resolution of the molecular diagrams of Fig. 6

A more complicated density redistribution pattern is observed in Fig. 6b. The strongest relocations are again observed in the atomic *core*-regions around the two nuclei dominated by the spin-paired 1s electrons, where turning-on the Coulomb correlation should indeed be most felt. It should be observed that these horizontal correlation effects polarize the atomic cores away from the triple-bond electrons. The lone-electron pair regions are seen to gain electrons at large distances from the nuclei at the expense of the valence regions less distant from the bond region. Indeed, the spin-paired valence electrons of the lone pairs are effectively Fermi-correlated by the spin-like electrons of the triple bond so that an extra switching-on of the Coulomb correlation exerts a smaller influence upon them. The average effect in the region of the bond-charge accumulation due to both σ and π bonds is also observed to be a slight lowering of the electron density. This density depletion can be also rationalized in terms of the strong exchange correlation between different bonding MO localized in this area, already present at the UHF level of theory. We also observe in this profile an "*inductive*" effect of the regions of positive horizontal density displacement being followed by regions of the negative shift in the electron density.

Let us now turn to the heteronuclear diagrams shown in the right column of Fig. 6. The LiH horizontal profile again exhibits an extra concentration of the electron density around the nuclei at the expense of the bonding and non-bonding regions, as in H_2. Notice, however, that the negatively charged bonded hydrogen is predicted to receive relatively more than its positively charged bond partner so that the horizontal Coulomb correlation displacement *increases* the UHF charge separation. This is contrary to the vertical Coulomb correlation influence seen in the Fig. 5b, which acted in the opposite direction towards a slight moderation of the UHF net AIM charges.

A reference to Fig. 6d indicates that the bonded fluorine atom in HF undergoes a similar charge redistribution as that observed for the bonded nitrogen in N_2, particularly in the core region, while the area in the vicinity of the proton gains electrons as in H_2 and LiH. Around the H–F bond this horizontal Coulomb correction is seen to shift electrons from the hydrogen to fluorine, thus again strengthening the UHF charge separation, contrary to the vertical moderating influence observed in Fig. 5c.

An opposite overall effect is detected in the most ionic LiF bond profile with the fluorine atom on average losing electrons and the bonded lithium atom gaining electrons. This horizontal Coulomb correlation influence partly moderates the magnitude of the UHF net AIM charges, thus acting in-phase with the vertical pattern of Fig. 5d.

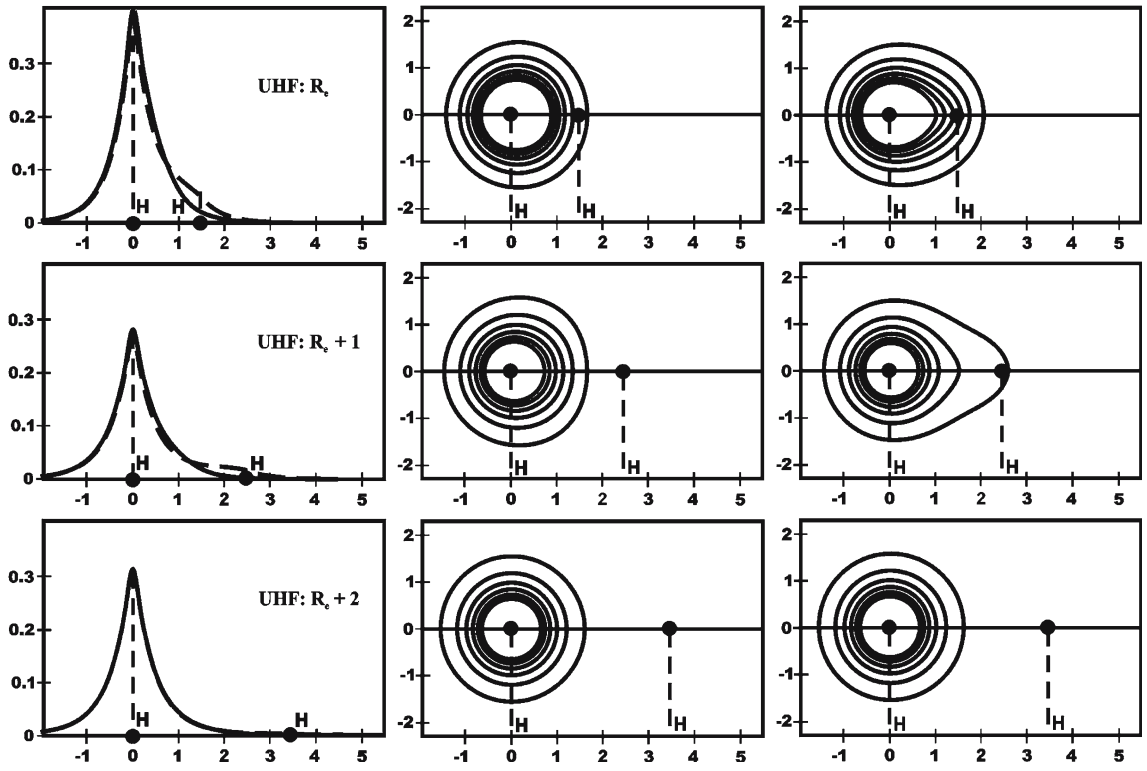

Fig. 8 Variations with increasing internuclear distance (a.u.) of the UHF electron densities of the one- and two-electron stockholder AIM in H_2, as reflected by the bond density profiles (*first column*) and the contour maps (*other two columns*). The Hirshfeld density pieces are shown in *Columns 1* (*solid lines*) and *2*, while the two-electron stockholder AIM are displayed in *Columns* 1 (*broken lines*) and *3*. The same convention is used in Figs. 9,10,11,12, and 13 (DZVP basis set)

Finally, in Fig. 7 these overall Coulomb correlation "horizontal" influences on the molecular electron densities of diatomic molecules have been resolved into the corresponding Hirshfeld AIM components. The figure shows changes in the electron distribution of the 1-*S* bonded atoms obtained from the ground-state density in the UMP2 approximation relative to their analogs derived from the molecular UHF electron density for the same (UHF optimum) internuclear distance.

It follows from Fig. 7a that the dominant horizontal effect of the Coulomb correlation on the density of the Hirshfeld hydrogen in H_2 is located in the region around the nucleus, giving rise to a more compact (contracted) electron distribution. Another distinct but relatively smaller effect is observed in the bonding region and around the nucleus of the other atom. This effect confirms our earlier conjecture from the 2-*S* diagrams for H_2 that an inclusion of the Coulomb correlation effects makes the stockholder hydrogens a bit more bonding in character.

The N_2 plots (Fig. 7b) are seen to slightly diminish their electron density in the lone-pair region, occupied by the nonbonding $2s–2p_\sigma$ hybrid, and to a less extent in the bonding region between the two nuclei. They also exhibit a strong core polarization. This pattern shows that the horizontal correlation effects slightly moderate some excess bonding character determined in the UHF approximation.

A similar trend is observed in the fluorine plot of Fig. 7d. The electron distribution of the bonded F in HF is seen to become slightly less diffused, when the Coulomb correlation is turned on. Both atoms are seen to withdraw part of their bond charge, thus effectively lowering the covalent bond component relative to the UHF reference. However, each AIM is also seen to slightly increase its density in the valence region of its bond partner. Finally, in the LiF diagrams of Fig. 7e one detects the dominant reduction of the excess electron population on the bonded fluorine atom, which effectively lowers the ionic bond component.

A reference to both AIM plots of Fig. 7c shows that the horizontal Coulomb correlation slightly increases the Li→H CT relative to the UHF charge separation. Again, the AIM electron distributions become more contracted around the nuclei at the expense of both the bonding and non-bonding regions of the molecule.

3.4 Near-dissociation bond elongations

It is of interest to examine the evolution of the electron distributions of the information-theoretic AIM, when the chemical bond is elongated from the equilibrium value to the near-dissociation limit. First, we compare the reference UHF results, which can be regarded as equivalent to the exact-exchange-only UHF-KS DFT calculations.

The representative plots for H_2 and LiH are reported in Figs. 8 and 9. These diagrams imply a smooth transition of

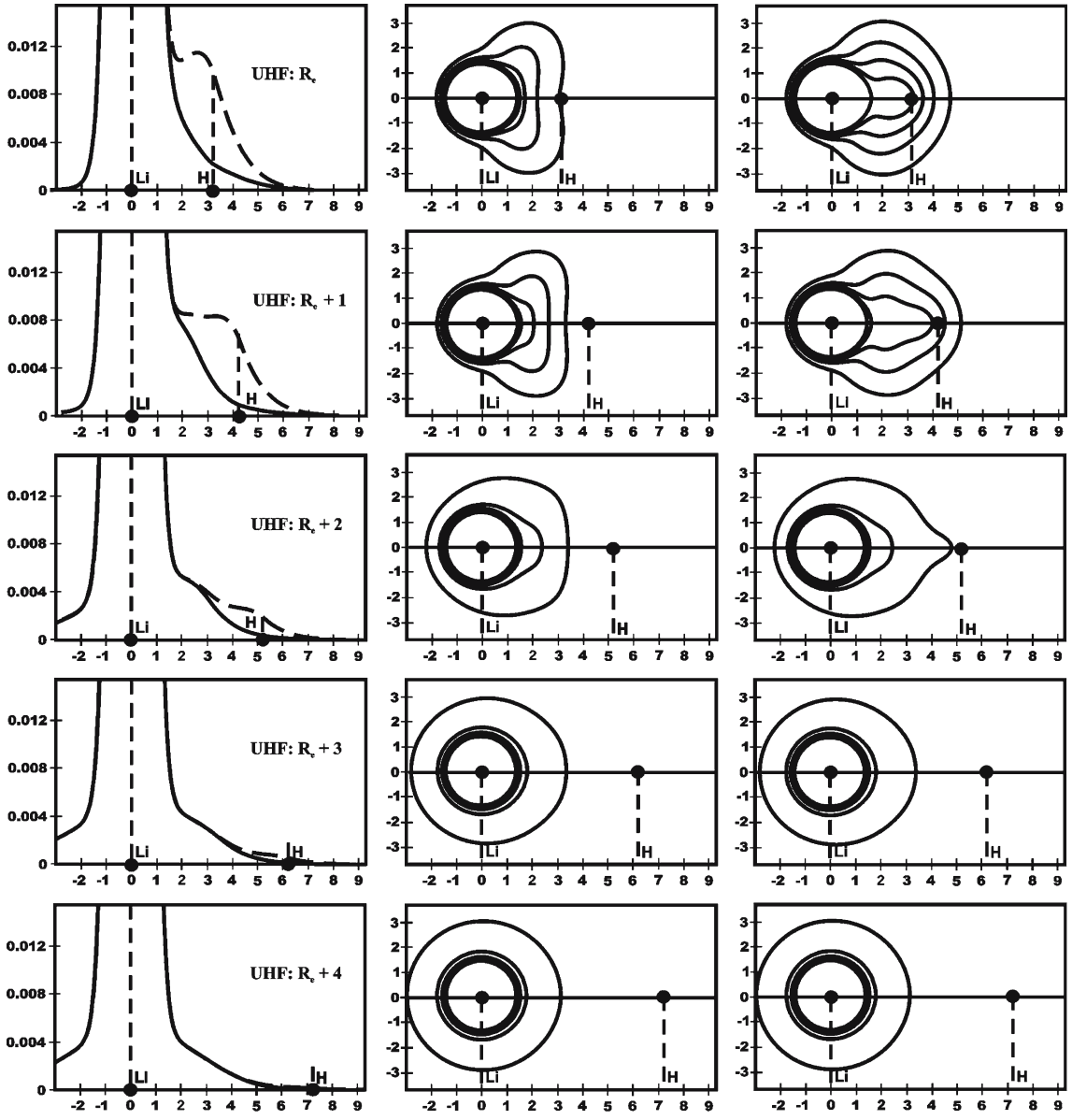

Fig. 9 Same as in Fig. 8 for Li in LiH

the electron densities of the bonded stockholder atoms into those of the corresponding free-atoms, when the chemical bond is elongated to the practically near-dissociation internuclear distance. At each stage the two-electron stockholder atoms are seen to exhibit a stronger and longer-lasting bond polarization towards the other atom in comparison to the one-electron (Hirshfeld) AIM. This bonded character can indeed be detected in the shapes of 2-*S* atoms at relatively higher bond length values in comparison to 1-*S* AIM, which assume the free-atom distribution with bond elongation faster.

Next, let us investigate the effect of approximations introduced in the DFT treatment of the Fermi holes, which characterize the exchange correlation in molecules, on the effective distributions of the bonded atoms obtained from the 2-*S* partition of the molecular electron densities. The two-electron probabilities from the (LDA, B3LYP) DFT calculations approximate the exact exchange holes resulting from the UHF theory. We shall now examine how these approximations affect the evolution of shapes of AIM during the bond dissociation. Clearly, the adequate representation of the "tails" of the x-holes, which ultimately determine the inter-atomic exchange correlation energy at large distances between dissociating atoms, may be expected to be crucial for a smooth transition from the bonded (*promoted*) atoms to the isolated (*separated*) atoms of the dissociation limit.

In Figs. 10 and 11 the evolution of the one- and two-electron stockholder AIM in the H–H bond elongation process is examined, as predicted by the DFT calculations using the LDA and B3LYP functionals approximating the exchange–correlation energy. These plots should be compared with the

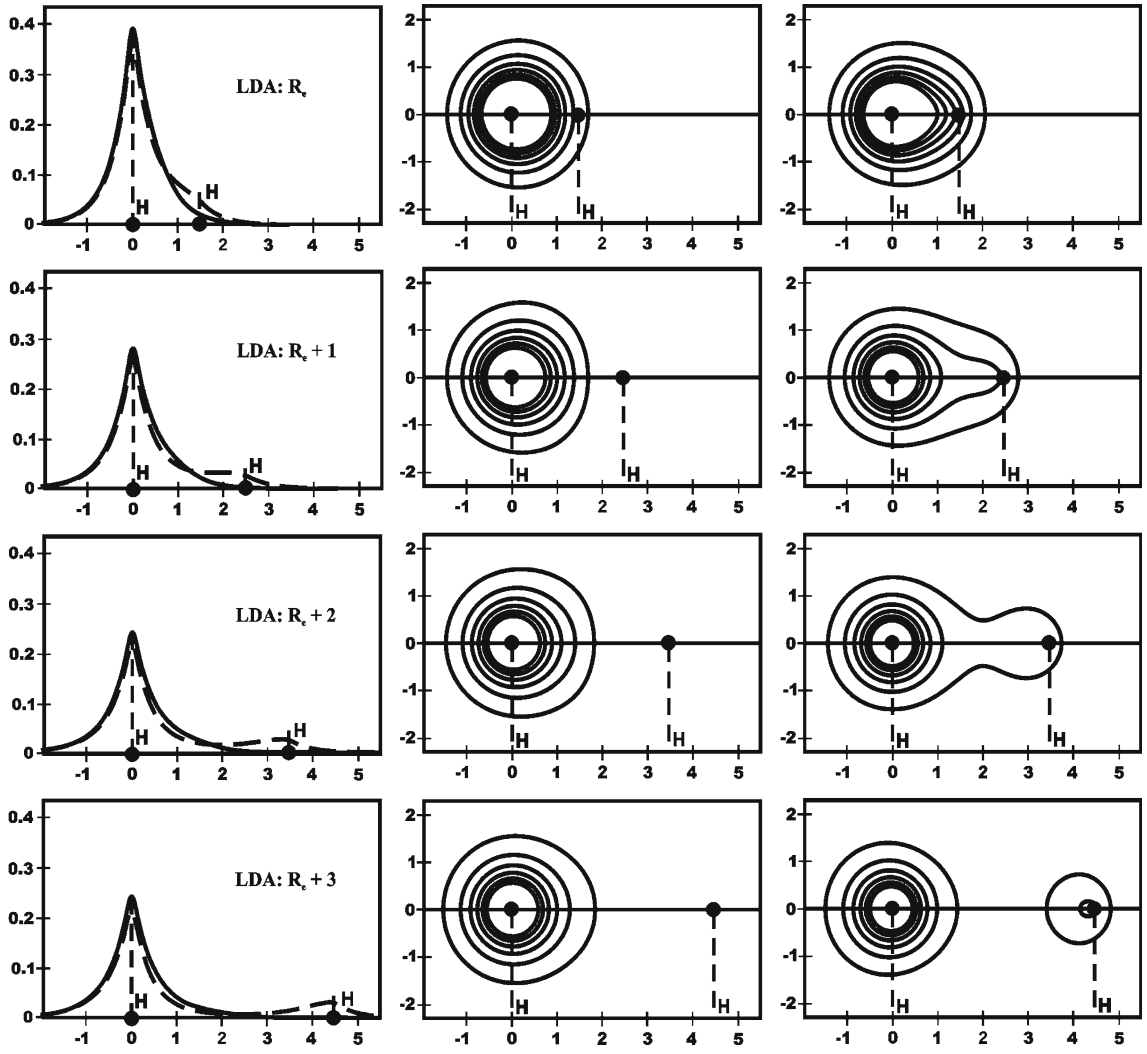

Fig. 10 Same as in Fig. 8 for the UHF-KS scheme based upon the LDA approximation of DFT

corresponding reference (UHF) diagrams shown in Fig. 8. It should be emphasized, however, that in heteronuclear diatomics, the adopted variants of DFT calculations give rise to the ionic pair in the dissociation limit instead of the neutral atoms. This is because the LDA and B3LYP functionals do not reproduce the N-discontinuities of the effective and chemical potentials, which are properly taken into account by the orbital-density functionals, e.g., the familiar Optimized Effective Potential (OEP) model, Krieger-Li-Iafrate (KLI) approximation, or the related exchange-only realization known as the Optimized Potential Model (OPM).

This comparison shows that in the two DFT calculations the Hirshfeld division scheme always leads to the *single-cusp* atomic density pieces, which eventually become identical with the free-atom densities at large internuclear distances.

This is no longer the case in the 2-S partition scheme, where the most approximate LDA variant is seen in Fig. 10 to give rise to the two-cusp feature in the bonded hydrogens for near-dissociation bond lengths. At large distances between atoms the more exact B3LYP functional is seen in Fig. 11 to remedy this incorrect prediction of the LDA theory, although a near-cusp shoulder can still be observed at the intermediate internuclear separation of the second row of Fig. 11.

This sensitivity of the two-electron stockholder partition with respect to the quality of the molecular two-electron density is more strongly demonstrated in the corresponding plots for LiH (Figs. 12, 13). These DFT results should be compared with the reference UHF electron densities of Fig. 9. Only Li plots are shown in Figs. 12 and 13, since the bonded hydrogen atoms have been found to be relatively insensitive to the quality of the approximate representations of the exchange-effects with both one- and two-electron stockholder divisions predicting almost identical hydrogen atoms in the molecule.

In the LDA approximation the two-cusp feature of the 2-S Li atom can be clearly seen already at the equilibrium bond length. This qualitative feature of the atomic electron density is seen to be relatively enhanced at larger distances between the two atoms. This somewhat unphysical artifact of the LDA

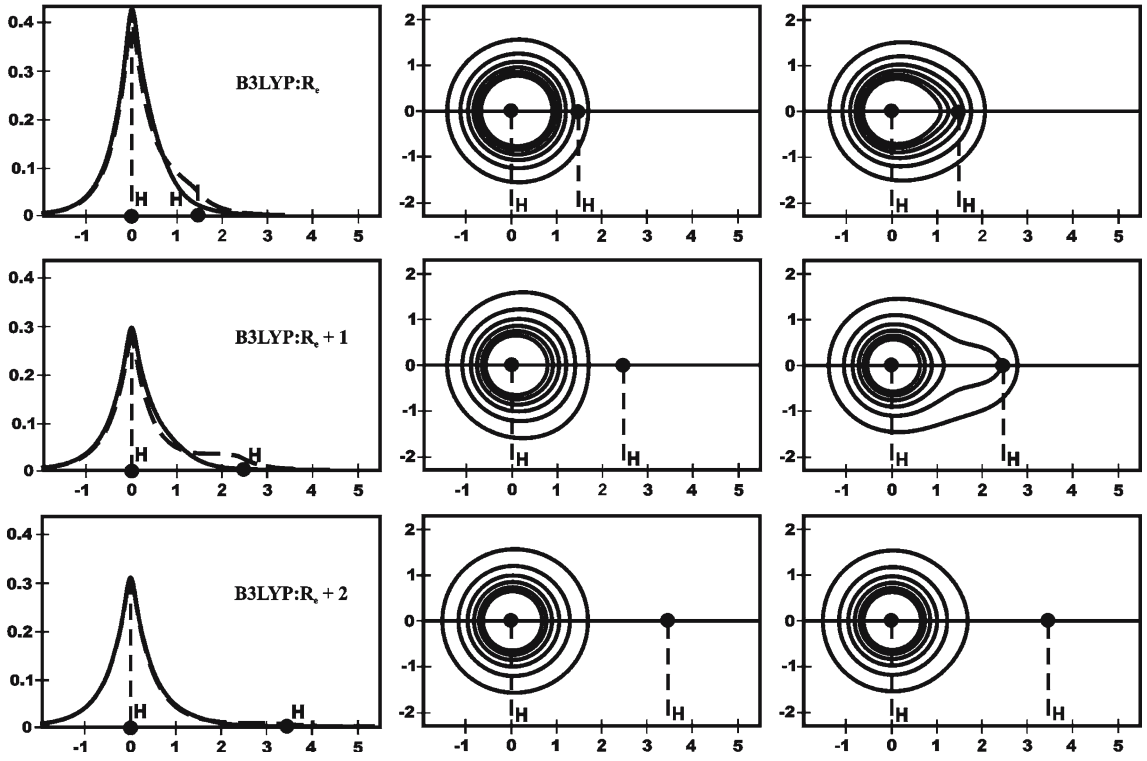

Fig. 11 Same as in Fig. 8 for the B3LYP exchange–correlation energy functional of DFT

approximation is remedied at large internuclear separations by the less approximate B3LYP DFT calculations using the density-gradient functional (see Fig. 13), although it can still be detected at intermediate bond elongations.

One can conclude from these illustrative results that a meaningful description of the two-electron stockholder atoms close to the bond dissociation can be obtained only from calculations in which the tails of correlation holes are realistically represented. The above illustrative results clearly show that the LDA of DFT does not satisfy this requirement, leading to the unphysical two-cusp densities of bonded atoms at large internuclear distances. In this regard the UHF results or the orbital-dependent exchange–correlation energy functional schemes of DFT, e.g., the OEP/KLI approximation, or the related exchange-only case known as the OPM, which in principle represents the exact UHF-KS scheme, should all provide an adequate description of the evolution of the effective one-electron densities of the 2-S AIM in the bond dissociation processes.

4 Cluster components of the two-electron stockholder AIM in diatomics

Let us examine for representative diatomics $M = AB$ the "diagonal" (one-center) and "off-diagonal" (two-center) components of the AIM two-clusters, $\{\rho^S_{\alpha\beta}(\boldsymbol{r},\boldsymbol{r}') = N(N-1)\, p^S_{\alpha\beta}(\boldsymbol{r},\boldsymbol{r}')\}$ [Eqs. (3), (4)] of the two-electron stockholder (2-S) AIM which we have introduced in Sect. 2. In order to visualize their contributions to the effective one-electron distribution of bonded atoms [Eq. (8)], we shall generate the bond-axis profiles of the partly integrated components of Eq. (7):

$$\rho^{\text{eff}}_{\alpha\beta}(\boldsymbol{r}) = \int \rho^S_{\alpha\beta}(\boldsymbol{r},\boldsymbol{r}')\mathrm{d}\boldsymbol{r}', \quad \alpha,\beta = (A,B). \tag{12}$$

As explicitly indicated in Eqs. (3) and (4) these cluster contributions are defined by the stockholder fractions $\{d^S_{\alpha\beta}(\boldsymbol{r},\boldsymbol{r}')\}$ of the molecular-pair density $\rho_2(\boldsymbol{r},\boldsymbol{r}')$,

$$\rho^S_{\alpha\beta}(\boldsymbol{r},\boldsymbol{r}') = d^S_{\alpha\beta}(\boldsymbol{r},\boldsymbol{r}')\rho_2(\boldsymbol{r},\boldsymbol{r}'), \tag{13}$$

which are uniquely determined by the free-atom distributions describing the promolecular reference. They represent the two-electron conditional probabilities $\{\pi^S(\alpha,\beta|\boldsymbol{r},\boldsymbol{r}')\}$ of Eq. (5), the normalization of which involves the summation over AIM labels α and β (variables) for the fixed electron positions (parameters), $\sum_\alpha \sum_\beta \pi^S(\alpha,\beta|\boldsymbol{r},\boldsymbol{r}') = 1$. As we have already observed in Sect. 2, the two-cluster density components can be alternatively viewed as the (cluster-independent, unbiased) molecular *enhancement* [Eq. (4)] of the corresponding promolecular two-cluster distributions $\{\rho^0_{\alpha\beta}(\boldsymbol{r},\boldsymbol{r}') = N(N-1)p^0_{\alpha\beta}(\boldsymbol{r},\boldsymbol{r}')\}$,

$$w_2(\boldsymbol{r},\boldsymbol{r}') = \rho_2(\boldsymbol{r},\boldsymbol{r}')/\rho^0_2(\boldsymbol{r},\boldsymbol{r}') \cong 1 \tag{14}$$

which give rise to the promolecular pair-density $\rho^0_2(\boldsymbol{r},\boldsymbol{r}') = \sum_\alpha \sum_\beta \rho^0_{\alpha\beta}(\boldsymbol{r},\boldsymbol{r}')$. In the preceding equation we have indicated that the molecular pair-density strongly resembles

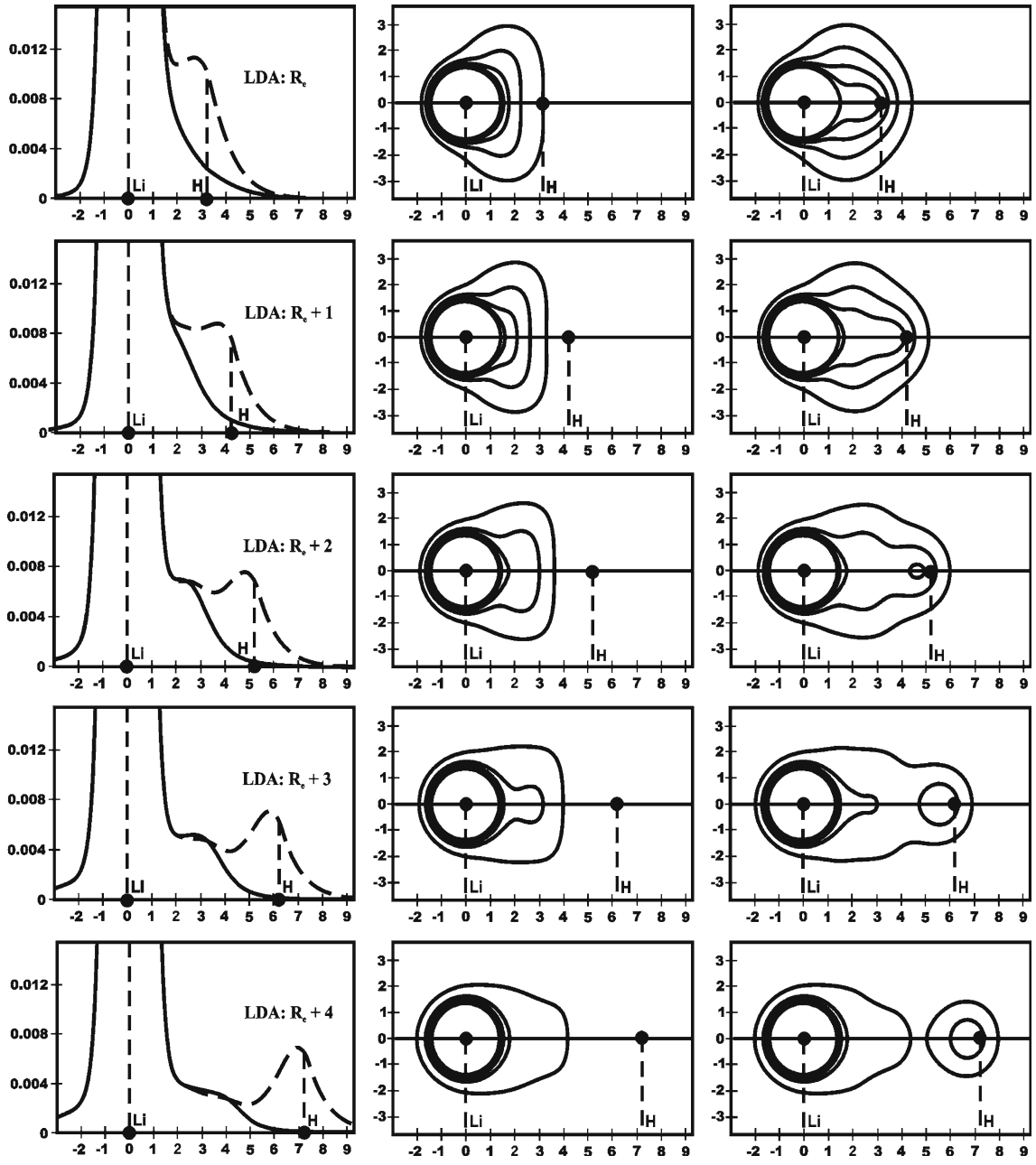

Fig. 12 Same as in Fig. 9 for Li in LiH and the LDA approximation of DFT

that of the promolecule. The associated two-electron probability distributions $\{p^0_{\alpha\beta}(\boldsymbol{r},\boldsymbol{r}')\}$ satisfy the promolecular normalization:

$$\sum_\alpha \sum_\beta \iint p^0_{\alpha\beta}(\boldsymbol{r},\boldsymbol{r}')\,\mathrm{d}\boldsymbol{r}\,\mathrm{d}\boldsymbol{r}' \equiv \sum_\alpha \sum_\beta P^0_{\alpha\beta} = 1; \qquad (15)$$

here the *condensed* cluster probabilities in the promolecule, $\mathbf{P}^0 = \{P^0_{\alpha\beta}\}$ are given by the following expressions in terms of the overall numbers of electrons in the isolated constituent atoms $\{N^0_\alpha\}$ and that of the isoelectronic promolecule $(N^0 = \sum_\alpha N^0_\alpha = N)$:

$$P^0_{\alpha\alpha} = N^0_\alpha(N^0_\alpha - 1)/[N^0(N^0-1)];$$
$$P^0_{\alpha\beta} = N^0_\alpha N^0_\beta/[N^0(N^0-1)], \quad \alpha \neq \beta. \qquad (16)$$

Also of interest are the partial normalizations of the cluster two-electron probabilities:

$$\int p^0_{\alpha\alpha}(\boldsymbol{r},\boldsymbol{r}')\mathrm{d}\boldsymbol{r}' = [(N^0_\alpha - 1)/(N^0-1)]p^0_\alpha(\boldsymbol{r}), \qquad (17)$$

$$\int p^0_{\alpha\beta}(\boldsymbol{r},\boldsymbol{r}')\mathrm{d}\boldsymbol{r}' = [N^0_\beta/(N^0-1)]p^0_\alpha(\boldsymbol{r}), \quad \alpha \neq \beta, \qquad (18)$$

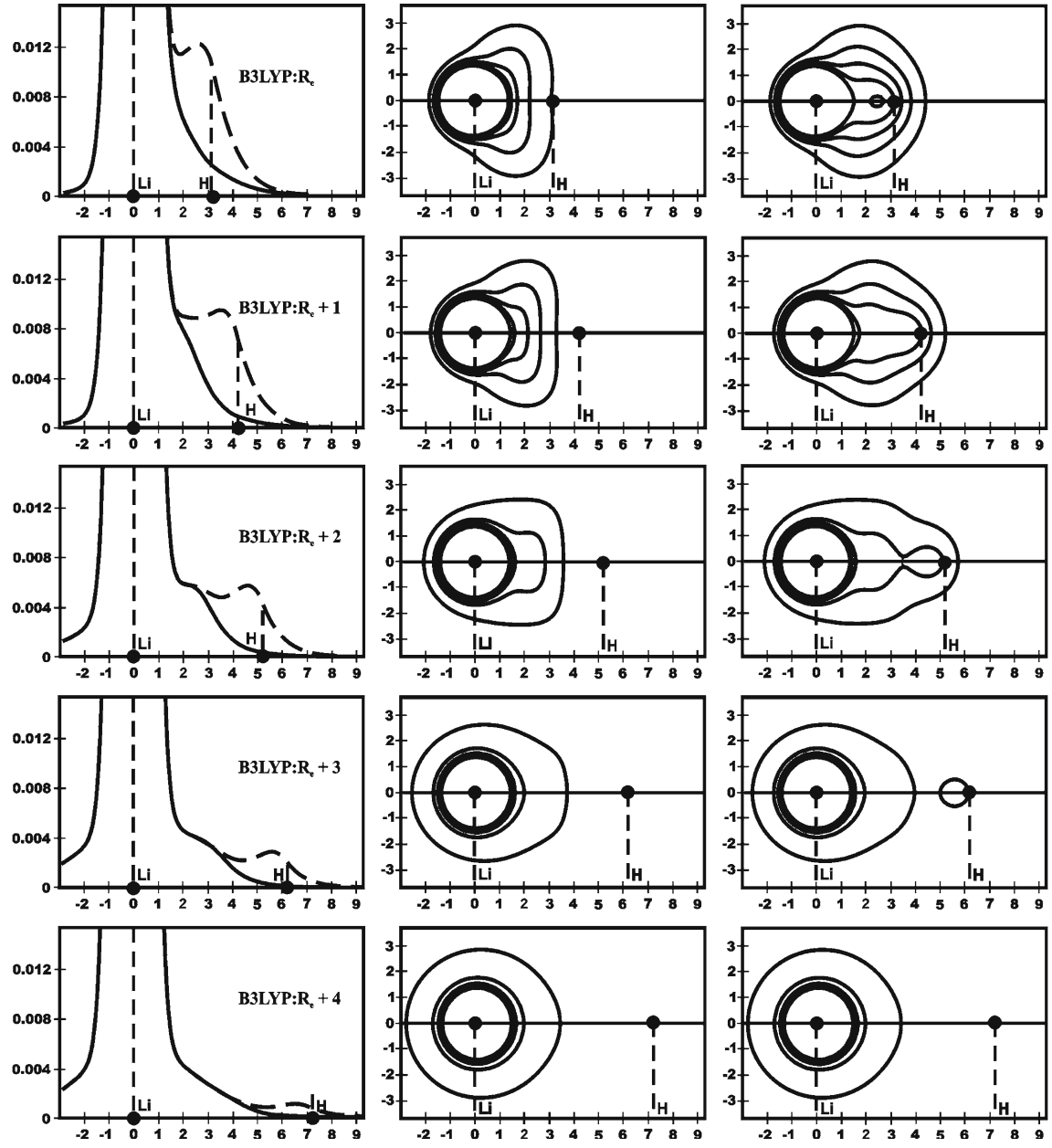

Fig. 13 Same as in Fig. 9 for Li in LiH and the B3LYP approximation of DFT

where the atomic one-electron distribution $p_\alpha^0(\boldsymbol{r})$ gives rise to the condensed atomic probability in the promolecule as a whole:

$$\int p_\alpha^0(\boldsymbol{r})\mathrm{d}\boldsymbol{r} = N_\alpha^0/N^0 \equiv P_\alpha^0, \quad \sum_\alpha P_\alpha^0 = 1. \tag{19}$$

Therefore, the off-diagonal ($\alpha \neq \beta$) two-cluster component is roughly separable:

$$p_{\alpha\beta}^S(\boldsymbol{r},\boldsymbol{r}') \cong p_\alpha^0(\boldsymbol{r})p_\beta^0(\boldsymbol{r}'), \tag{20}$$

thus giving rise to the α-cusped effective off-diagonal contribution due to the other atom β, to the density distribution of αth AIM:

$$p_{\alpha\beta}^{\mathrm{eff}}(\boldsymbol{r}) \cong p_\alpha^0(\boldsymbol{r}')\int p_\beta^0(\boldsymbol{r}')\mathrm{d}\boldsymbol{r}' = [N_\beta^0/(N^0-1)]p_\alpha^0(\boldsymbol{r}). \tag{21}$$

Clearly, the promolecular dominance of the molecular diagonal component,

$$p_{\alpha\alpha}^S(\boldsymbol{r},\boldsymbol{r}') \cong p_{2,\alpha}^0(\boldsymbol{r},\boldsymbol{r}'), \tag{22}$$

will also generate the effective contribution proportional to $p_\alpha^0(\boldsymbol{r})$:

$$p_{\alpha\alpha}^{\mathrm{eff}}(\boldsymbol{r}) \cong \int p_{2,\alpha}^0(\boldsymbol{r},\boldsymbol{r}')\mathrm{d}\boldsymbol{r}' = [(N_\alpha^0-1)/(N^0-1)]p_\alpha^0(\boldsymbol{r}). \tag{23}$$

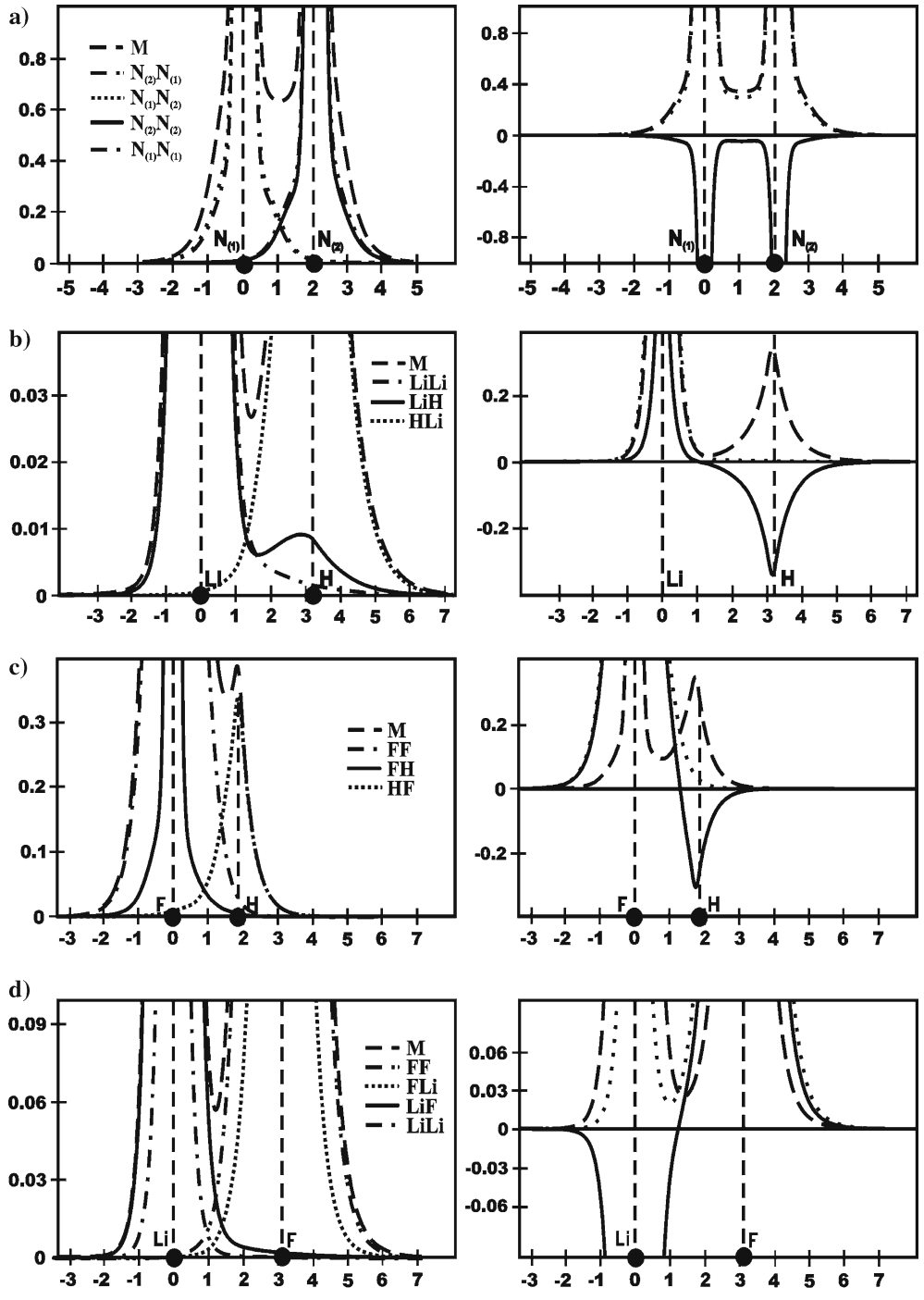

Fig. 14 *Left column*: the bond axis profiles of the two-cluster components $\{\rho^{\rm eff}_{\alpha\beta}(\boldsymbol{r})\}$ of the 2-S AIM in: N_2 (**a**), LiH (**b**), HF (**c**), and LiF (**d**). *Right column* shows the corresponding sums of the diagonal (*dotted line*) and off diagonal (*broken line*) components, $C(\boldsymbol{r}) \equiv \rho^{\rm eff}_{\alpha\alpha}(\boldsymbol{r}) + \rho^{\rm eff}_{\beta\beta}(\boldsymbol{r})$ and $D(\boldsymbol{r}) \equiv \rho^{\rm eff}_{\alpha\beta}(\boldsymbol{r}) + \rho^{\rm eff}_{\beta\alpha}(\boldsymbol{r})$, respectively, while the *solid line* represents the difference $C(\boldsymbol{r}) - D(\boldsymbol{r})$ [UHF-KS(LDA) scheme, DZVP basis set]

Hence, both $p^{\rm eff}_{\alpha\beta}(\boldsymbol{r})$ and $p^{\rm eff}_{\alpha\alpha}(\boldsymbol{r})$ components can be expected to strongly resemble the indicated fractions of the promolecularly normalized free-atom distribution $p^0_\alpha(\boldsymbol{r})$:

$$p^{\rm eff}_{\alpha\alpha}(\boldsymbol{r}) + p^{\rm eff}_{\alpha\beta}(\boldsymbol{r}) \cong p^0_\alpha(\boldsymbol{r})(N^0_\alpha - 1 + N^0_\beta)/(N^0 - 1) = p^0_\alpha(\boldsymbol{r}). \quad (24)$$

These expectations are supported by the numerical results for the representative diatomics, H_2, LiH, HF, LiF, and N_2, which are reported in Figs. 14, 15, 16. These figures summarize the 2-S partitioning of the molecular two-electron densities obtained from the UHF-KS orbitals resulting from the LDA approximation (DZVP basis set). These calculations

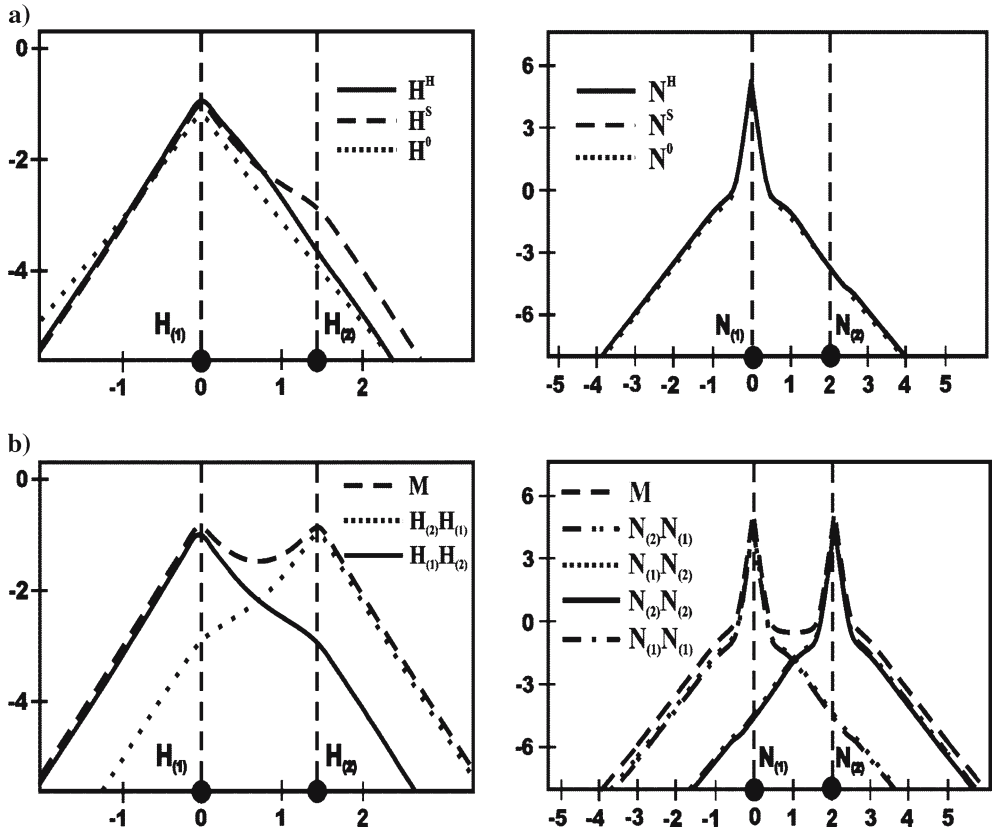

Fig. 15 A comparison of the logarithmic plots of the electron density profiles along the bond axis of the isolated (^{0}), 1-S (^{H}), and 2-S (^{S}) atoms (Part **a**), and of the molecular (M) and the AIM two-cluster components of the effective atomic densities (Part **b**), in H_2 (*left column*) and N_2 (*right column*) [UHF-KS(LDA) scheme, DZVP basis set]

can be regarded as being practically equivalent to the UHF approximation, which exactly takes into account the exchange (Fermi) correlation between electrons and completely neglects the many-body effects due to the Coulomb interaction. In Fig. 17 the influence of the Coulomb correlation estimated using the UMP2 method (DZV basis set), is examined.

Since in the isolated hydrogen atom (one-electron system) $p^0_{2,\mathrm{H}}(\boldsymbol{r},\boldsymbol{r}') = 0$, the diagonal component of the 2-S division identically vanishes. Therefore, the effective one-electron distribution of the 2-S hydrogens in a diatomic molecule, which are referenced to the isolated (neutral) atom, has only the off-diagonal cluster contribution, shown in Figs. 1, 2, 3, and 4 as well as in the logarithmic plot of the left panel of Fig. 15. It follows from the approximate relation (21), that this term gives rise to $\rho^S_{\mathrm{H}}(\boldsymbol{r}) \cong \rho^0_{\mathrm{H}}(\boldsymbol{r})$.

Thus, changes in the electron distribution of the bonded hydrogen due to the polarization and CT have to be reflected by the off-diagonal components linking the atom with its bond partners. This is particularly constraining in the LiH case [see Fig. 1b, right panel of Figs. 2b, 4c, 14b, 16 (left column)], where the negatively charged hydrogen has to accommodate the extra electron transfer from Li. The resulting CT "shoulder" is clearly visible in the $p^{\mathrm{eff}}_{\mathrm{LiH}}(\boldsymbol{r})$ profiles shown in Figs. 14b and 16c (left panel). It should be realized, however, that this artificial feature practically disappears in HF [Figs. 14c, 16c (medium column)], i.e., for the positively charged 2-S hydrogen, when it acts as the net electron donor. This is because the inflowing charge on F can be freely accommodated by the open diagonal (ionic) channel on fluorine atom, $p^{\mathrm{eff}}_{\mathrm{FF}}(\boldsymbol{r})$. The other reason for this difference is the three times higher number of electrons in F compared to Li. Nevertheless, in the logarithmic plot of panel c in the middle column of Fig. 16, one still detects a minor shoulder in the $p^{\mathrm{eff}}_{\mathrm{FH}}(\boldsymbol{r})$ profile at the proton position.

In the homonuclear N_2 system [Figs. 14a, 15b (right panel)] the diagonal ("ionic") and off-diagonal ("covalent") contributions to a given bonded nitrogen atom are seen to be almost equal with the exception of the 1s core regions around the nuclei, where the covalent terms dominate. This feature is clearly reflected in the right panel of Fig. 14a, where the balance between the overall diagonal and off- diagonal components is investigated.

This overall equality of both these contributions in the chemically most important valence-shell, identifies the purely covalent matching between the diagonal and off-diagonal-pair-density components of the 2-S AIM. It is reminiscent of the equal share of the *ionic* and *covalent* VB-structures in the minimum basis set SCF MO description of the purely covalent chemical bond in H_2.

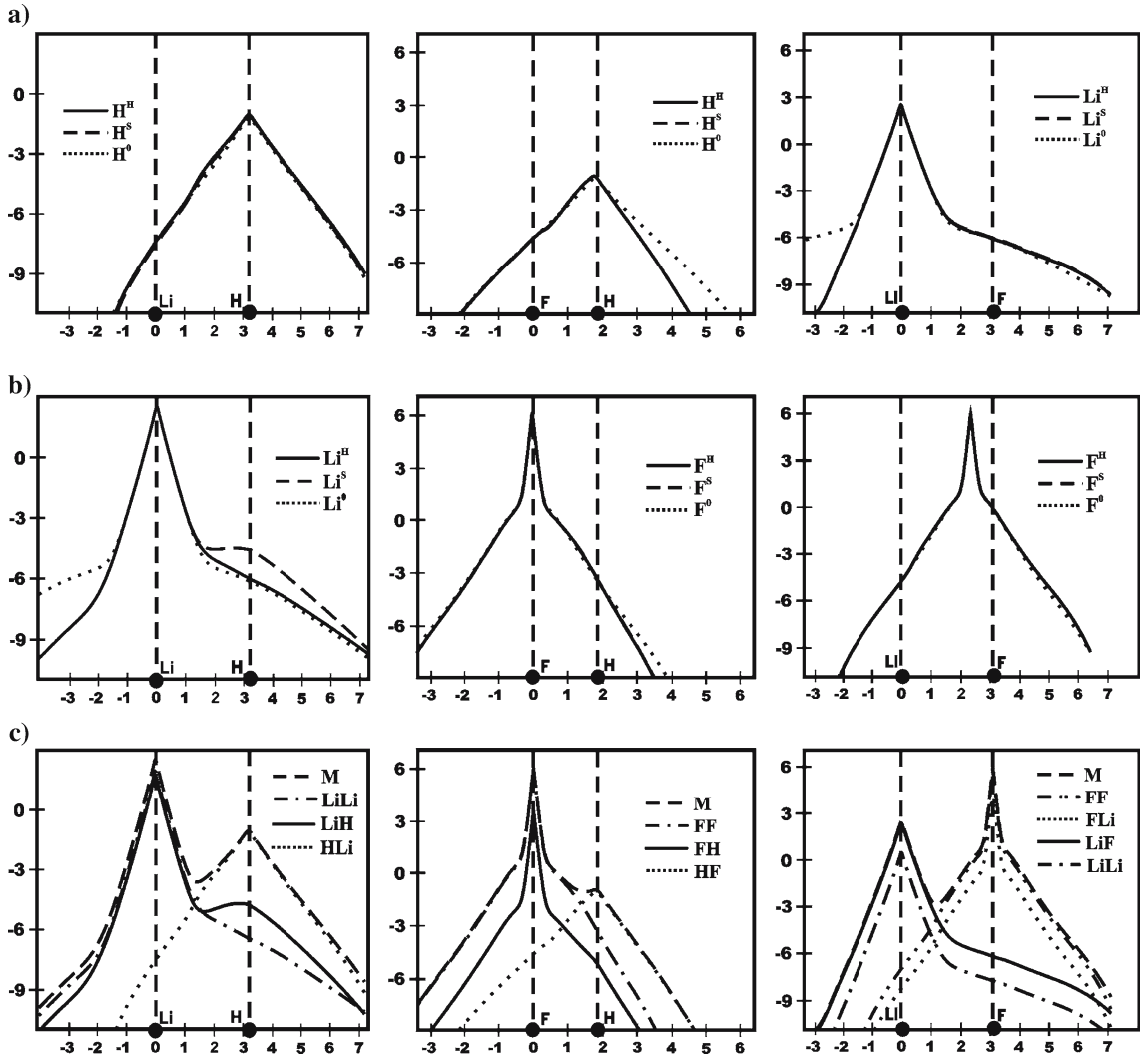

Fig. 16 A comparison of the logarithmic plots of the electron density profiles along the bond axis of the isolated (^{0}), 1-S (^{H}), and 2-S (^{S}) atoms (**a**, **b**), and of the molecular (M) and the AIM two-cluster components of the effective atomic densities (**c**), in LiH (*left column*), HF (*middle column*), and LiF (*right column*) [UHF-KS(LDA) scheme, DZVP basis set]

The difference between the overall diagonal and off-diagonal density contributions in heteronuclear diatomics clearly reflects the bond ionicity and the CT between the bonded 2-S AIM. This is most transparently seen in LiF, in the right panel of Fig. 14d, where both covalent and ionic channels of both atoms are open. The overall off-diagonal contribution is found to dominate the donor (Li) atom region, while the opposite trend is detected in the acceptor (F) atom. The difference (solid line) plot directly reflects the Li→F CT. A similar H→F CT pattern can be detected in HF (see the right panel of Fig. 14c), for which the open diagonal channel on fluorine can accommodate the inflowing charge donated by the hydrogen.

The opposite trend observed in LiH is not representative of this general balance, since this is the artifact of the closed ionic (diagonal) channel on the acceptor hydrogen atom. Indeed, the net inflow of electrons to the bonded, acceptor 2-S hydrogen cannot be accommodated through the off-diagonal (H, Li) component, which strongly resembles the isolated hydrogen density. It can be absorbed only in the other (Li, H) off-diagonal component, which is attributed in the 2-S division scheme to the bonded lithium atom. This artificially creates the unphysical dominance of the overall "covalent" density component in the hydrogen region and the net "acceptor" difference plot in the lithium region.

In Table 1 we have listed the net AIM charges for the constituent 1-S (Hirshfeld) and 2-S stockholder atoms in these three heteronuclear diatomics. It follows from the table that with the increasing number of electrons the differences between the net charges of the 1-S and 2-S AIM gradually disappear. The largest deviation is observed for LiH for the reasons discussed above.

The two sets of the AIM charges qualitatively reflect the chemically expected bond polarization due to the electronegativity difference exhibited by the isolated atoms. A general rule emerging from this comparison is that the 2-S

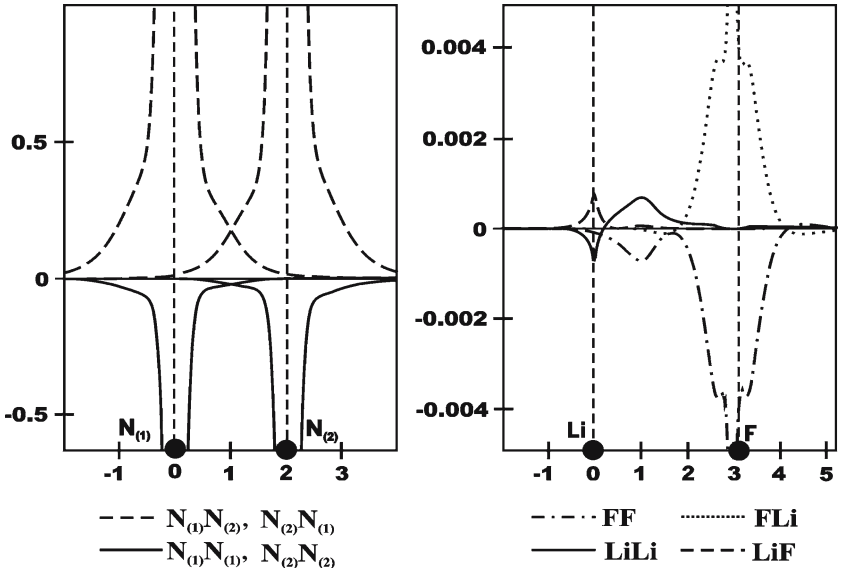

Fig. 17 The effect of the extra Coulomb correlation on the exchange-only correlated two-cluster components of the effective AIM densities in N_2 (*left panel*) and LiF (*right panel*)

AIM, which effectively contain the Fermi correlation effects, exhibit less charge separation in comparison to the 1-S (Hirshfeld) atoms. For example, the 2-S Li[LiH] exhibits distinctly less positive net charge, $q^S_{\rm Li} = 0.24$, compared to the 1-S $\rm Li^H$ [LiH], $q^H_{\rm Li} = 0.35$, which accords with the closed diagonal (acceptor) channel on the bonded hydrogen. In the two remaining diatomic molecules this difference is seen to be substantially reduced.

In the logarithmic plots of Figs. 15 and 16 we have examined in more detail the valence-shell decays of the effective electron densities of the 2-S bonded atoms in homonuclear diatomics, and their AIM two-cluster components. These plots are compared against the corresponding free- and Hirshfeld-atom densities and the molecular electron density.

The diagrams for the homonuclear diatomics (Fig. 15) confirm the molecular character of the bonded hydrogen atoms resulting from both divisions, with the constant decay rate at large distances, determined by the molecular ionization potential. In Fig. 15a the extra-bonding character of the 2-S hydrogen atoms in H_2, relative to the Hirshfeld analogs, is now pronounced. It should be observed that the differences between the 1-S and 2-S nitrogen atoms in N_2 practically disappear also for the low values of the electron densities emphasized by these logarithmic plots. The approximate equality of the ionic (diagonal) and covalent (off-diagonal) density contributions of the 2-S nitrogens marking the purely covalent, multiple bond in N_2, is seen to hold also at these valence regions of low electron density.

Similar conclusions follow from examining the logarithmic density profiles of Fig. 16, for the three representative heteronuclear diatomics: LiH (left column), HF (medium column), and LiF (right column). The H[LiH] logarithmic plots of the Hirshfeld and 2-S AIM shown in the upper panel, exhibit only minor differences at the low density region in comparison to the free hydrogen atom while the extra density polarization of the Li valence 2s electron from the nonbonded region towards the hydrogen can be detected in the medium panel of the left column in the figure. It is more pronounced in the two-electron stockholder lithium due to the off-diagonal (covalent) LiH component seen in the lowest panel. The density decay of the polarized LiH molecule is seen to be governed by the two components due to softer Li atom: $\{\rho^{\rm eff}_{\alpha{\rm Li}}(\boldsymbol{r}), \alpha = {\rm H, Li}\}$. The CT polarization of the bonded hydrogen in HF is clearly seen in the upper panel of the middle column. No substantial differences between the 1-$S(H)$ and 2-$S(S)$ constituent atoms are observed for this diatomic consisting of two *hard* atoms, which generate the partly ionic bond with a strong covalent component. A typical behavior of the logarithmic profiles for the electron donor (Li) and acceptor (F) is also seen in the third column of the figure, with the bonded lithium exhibiting a strong polarization of its valence electron density towards fluorine. Both one- and two-electron divisions give rise to practically identical sets of AIM density profiles at the low density regions emphasized by the logarithmic plots.

In Fig. 17 we have examined the effect of the Coulomb correlation on the two-cluster components of the effective one-electron distributions of constituent AIM in N_2 and LiF. As intuitively expected, in the homonuclear diatomic (left panel) the diagonal (ionic) contributions, corresponding to events of finding two electrons on the same atom, are lowered in the immediate vicinity of the nuclei, where the accumulation of electrons is the highest. This is accompanied by a strong increase of the off-diagonal (covalent, delocalization) components in these two nuclear regions due to an increased sharing of the bonding electrons by the two AIM. In other words, the Coulomb correlation lowers the one-center ionic terms in favor of the two-center covalent contributions to the

effective electron density of the 2-*S* bonded AIM. A reference to the right panel in the figure shows that this electron correlation also moderates the charge separation resulting from the exchange-only approximation. Indeed, the FF profile implies a slight decrease of the effective electron density on F resulting from the fluorine one-center two-electron contribution. This diagonal component also implies a lowering of the density in the bond region, near the Li atom, which is compensated by the lithium one-center contribution. We also observe a complementary increase in the two-center FLi profile on the fluorine due to the Coulomb correlation, a direct manifestation of an increased covalency of the Li–F bond, i.e., a slightly higher sharing of the valence electrons between the bonding partners.

This analysis shows that an inclusion of the "vertical" coulomb correlation moderates a somewhat inflated charge separation of the "independent-particle" (Hirshfeld) stockholder division of the molecular electron density. The dominating correlation effect in the 2-*S* AIM distributions results from the exchange (Fermi) correlation contribution, with the remaining Coulomb correlations introducing only a minor modification of the exchange-only interpretation of the two-electron joint probabilities, which gives rise to qualitatively the same net AIM charges.

5 Conclusion

We have compared the bonded atoms resulting from the "stockholder" partitioning of the molecular one- and two-electron distributions. The one-electron case represents the familiar Hirshfeld partition, which was recently shown to follow from the minimum cross-entropy principle of the IT using the free-atom, promolecular reference. Applying this missing-information principle to the more general problem of dividing the molecular joint two-electron distribution, generates an extension of the one-electron stockholder principle of Hirshfeld to the associated two-electron rule for dividing the molecular electron pair-probabilities (densities) into the one- and two-center AIM contributions. When the two schemes are applied to the same molecular electron density, the two-electron stockholder scheme takes into account the *vertical* electron correlation effects.

We have thus compared the one-electron densities of the 1-*S* and 2-*S* AIM, which result from the same density of the molecule as a whole. The electron densities of bonded atoms in H_2 and LiH show that the two-electron stockholder treatment emphasizes more strongly the bonding region of the atomic distribution in comparison to the one-electron (Hirshfeld) scheme, giving rise to a more pronounced polarization of the atom towards its bond partner. However, this subtle difference was found to fast disappear with the increasing number of electrons in the molecular system. For heavier atoms the electron densities and probability distributions of the 1-*S* and 2-*S* AIM are practically identical.

The adequate two-electron density components of nearly separated AIM can be obtained only from calculations using a correct description of the inter-atom electron correlation effects. The most approximate UHF-KS(LDA) DFT calculations have been shown to give rise to a qualitatively incorrect, two-cusp AIM densities for the near-dissociation bond-elongations. This shortcoming was partly remedied using the B3LYP functional, which in the 2-*S* division leads to a dissociation into the separated free atoms, in full agreement with the predictions of the UHF theory.

Therefore, the Hirshfeld atomic subsystems representing the optimum (equilibrium) molecular fragments resulting from the minimum entropy-deficiency principle, are not exactly unique in the IT since the two-electron stockholder division defines slightly different effective one-electron distributions of bonded atoms, which give rise to the same one-electron distribution. However, with these differences being found to be so minute for most of the many-electron constituent atoms, one can safely conclude that the promolecule-referenced two-electron division problem gives rise to practically identical sets of 1-*S* and 2-*S* AIM. This "*invariance*" property of the many-electron stockholder bonded atoms in the IT treatment additionally validates the wide use of the Hirshfeld atoms in crystallography and their several unique properties, which make them attractive concepts for interpretations in chemistry.

For illustrative diatomic molecules we have explored in some detail the *vertical* and *horizontal* Coulomb correlation influences on the atomic and molecular electron densities as well as their one- and two-center components of the 2-*S* division scheme. The diagonal (one-center) AIM-components of this partition measure the joint probability of finding two electrons on the same AIM, thus corresponding to the *ionic* valence structures of the VB theory of Heitler and London. Similarly, the two-center off-diagonal contributions, measuring the joint probabilities of finding two electrons on different bonded atoms, can be naturally associated with the *covalent* valence structures of the VB theory. In this perspective, the stockholder partitioning of the molecular two-electron densities provides a convenient theoretical framework for describing these two components of the chemical bond.

We have also observed in Sect. 4 that the purely covalent triple bond in N_2, in which all division channels are accessible, corresponds to almost equalized one- and two-center components, again in perfect analogy to the VB description. Therefore, one should associate a deviation from this balance as a reflection of the bond ionicity. A notable exception to this rule is provided by the 2-*S* hydrogen atoms originating from the one-electron free-atom reference, which participate in the molecular density only through the off-diagonal (H,α)-components.

Clearly, the density differences between two isoelectronic systems have to integrate to zero. This closure has indeed been used as an important verification of the numerical accuracy of the present calculations. However, the corresponding bond-profiles, e.g., of correlation density displacements in Figs. 6 and 7, can be partly misleading, since they neglect small contributions from the large volume at long distances

from the molecule, which compensate the dominating shifts in the vicinity of the nuclei. It should also be realized that such minute density changes due to horizontal and vertical correlation effects obviously must depend on the size and quality of the basis set. However, since the main goal of the present study was to examine differences between 1-*S* and 2-*S* AIM, we claim that the adopted DZV and DZVP basis sets are sufficient for this objective. The main effects due to the closed channels for electron relocations in 2-*S* hydrogen in a molecule and the near identity of the two sets of stockholder heavy atoms are invariant to basis set choice.

Another source of difficulty may potentially arise from using the UHF approximation in the bond-dissociation phenomena, for which the more advanced CI and coupled-cluster methods remove some artifacts of the UHF potential energy curves for elongated diatomics. We would like to stress again, however, that the UHF reference is crucial for separating the Coulomb correlation from the exchange effects, which is vital for the comparative character of the present analysis. Moreover, the main purpose of the present bond-elongation investigation is the final, near-separated-atom limit, which is correctly reached at the UHF level of theory.

Information theory provides a powerful tool for extracting chemical concepts from molecular densities and for dividing the molecular quantities, e.g., bond descriptors, into atomic contributions using the so-called probability partitioning rule [44]. The theory establishes the information-entropy representation of the molecular electronic structure, complementary to the energy representation of conventional quantum chemistry. The Hohenberg–Kohn variational principle of DFT can be transcribed as an equivalent information principle of the entropy representation [45], which parallels the maximum entropy principle of the ordinary thermodynamics. The information meaning of the electron-localization-function [46] has also been identified [47].

Acknowledgements This work was partly supported by the research grant from the Committee for Scientific Research in Poland (Grant No. 4T09A18324).

References

1. Bader RFW (1990) Atoms in Molecules. Oxford University Press, New York
2. Parr RG, Ayers PW, Nalewajski RF (2005) J Phys Chem A 109:3957
3. Hirshfeld FL (1977) Theor Chim Acta (Berl) 44:129
4. Nalewajski RF, Parr RG (2000) Proc Natl Acad Sci USA 97:8879
5. Nalewajski RF, Parr RG (2001) J Phys Chem A 105:7391
6. Nalewajski RF (2002) Phys Chem Chem Phys 4:1710
7. Nalewajski RF (2003) Chem Phys Lett 372:28, 375:196
8. Nalewajski RF (2003) Adv Quantum Chem 43:119
9. Nalewajski RF (2006) Information theory of molecular systems. Elsevier, Amsterdam
10. Fisher RA (1922) Philos Trans R Soc Lond 222:309
11. Fisher RA (1925) Proc Camb Philos Soc 22:700
12. Fisher RA (1959) Statistical methods and scientific inference, 2nd edn, Oliver and Boyd, London
13. Frieden BR (2000) Physics from the Fisher information - a unification. Cambridge University, Cambridge
14. Shannon CE (1948) Bell Syst Tech J 27:379, 623
15. Shannon CE, Weaver W (1949) The mathematical theory of communication. University of Illinois, Urbana
16. Abramson N (1963) Information theory and coding. McGraw-Hill, New York
17. Kullback S, Leibler RA (1951) Ann Math Stat 22:79
18. Kullback S (1959) Information theory and statistics. Wiley, New York
19. Jaynes ET (1957) Phys Rev 106:620, 108:171
20. Ash RB (1965) Information theory. Interscience, New York
21. Brillouin L (1956) Science and information theory. Academic, New York
22. Nalewajski RF (2003) J Phys Chem A 107:3792
23. Nalewajski RF (2002) Acta Chim Phys Debr 34,35:131
24. Nalewajski RF (2004) Ann Phys (Leipzig) 13:201
25. Nalewajski RF, Broniatowska E (2003) J Phys Chem A 107:6270
26. Nalewajski RF, Broniatowska E (2003) Chem Phys Lett 376:33
27. Nalewajski RF, Broniatowska E (2005) Int J Quantum Chem101:349
28. Nalewajski RF, Loska R (2001) Theor Chem Acc 105:374
29. Nalewajski RF, Świtka E (2002) Phys Chem Phys 4:4952
30. Nalewajski RF, Świtka E, Michalak A (2002) Int J Quantum Chem 87:198
31. Nalewajski RF (2000) J Phys Chem A 104: 11940
32. Nalewajski RF (2004) Mol Phys 102:531,547
33. Nalewajski RF (2005) Mol Phys 103:451
34. Nalewajski RF (2006) Mol Phys 104:365
35. Nalewajski RF (2004) Struct Chem 15:395
36. Nalewajski RF (2004) Chem Phys Lett 386:265
37. Nalewajski RF (2005) Theor Chem Acc 114:4
38. Nalewajski RF (2005) J Math Chem 38:43
39. Hohenberg P, Kohn W (1964) Phys Rev 136B:864
40. Kohn W, Sham LJ (1965) Phys Rev 140A:1133
41. Heitler W, London F (1927) Z Phys 44:455
42. Hettema H (2000) Quantum chemistry classic scientific paper. World Scientific, Singapore
43. London F (1928) Z Phys 455:46
44. Nalewajski RF (2006) Mol Phys 104:493
45. Nalewajski RF (2006) Mol Phys 104:255
46. Becke AD, Edgecombe KE (1990) J Chem Phys 92:5397
47. Nalewajski RF, Köster AM, Escalante S (2005) J Phys Chem A 109:10038